
Elastic Metamaterials for Radiofrequency Applications

Micro-electromechanical components harnessing the propagation of elastic waves at frequencies in the GHz range have become ubiquitous in radiofrequency systems. The most popular of these systems are mobile phones, initially developed for human-to-human communication with the first GSM phones in the late 1990s. Successive generations of communication systems have since then evolved towards an increasing amount of machine-to-machine data exchange. The fifth generation of mobile communication system (5G), whose deployment is termed in the 2020s, is heralded as the one delivering broadband Internet access to every wirelessly connected device. In such purely electrical systems, elastic wave resonant cavities have successfully established a niche in providing miniature, low loss, and fully passive resonators, which are used as frequency selection components in electronic circuits. Such elements are building blocks of low-loss band-pass filters, which in turn are key elements of the analog stages of radiofrequency transceivers, whose function is to select only the relevant portions of the radio spectrum and maintain noise levels for radio receivers to extremely low levels in order to ensure a high sensitivity.

This requirement for ever-increased filtering capabilities over the tiniest possible fingerprint has quite naturally led the phononic crystal research community to pay some interest to a potential transposition of the concepts related to phononic crystals, or, to a lower extent, to elastic metamaterials, to radio frequencies. The demonstrations in the audible or ultrasonic range of filters, waveguides or even multiplexers suggested the possibility to implement advanced signal processing functionalities over *phononic chips*, mirroring similar developments in photonics. This process was in addition significantly made easy by the already acute

understanding of dispersion engineering and Bragg band gaps in one-dimensional structures by RF filter designers. The use of periodical structures in electro-acoustic devices had indeed a long and fruitful history already. To quote but a few examples, surface acoustic wave (SAW) transducers and reflectors rely on periodical arrays of metal electrodes fulfilling the Bragg condition and the definitely mature solidly mounted bulk acoustic wave resonators (SMR) use a stack of alternating layers of materials with contrasting elastic constant and mass densities to confine bulk waves in a piezoelectric thin film.

The question was then to demonstrate the existence of two-dimensional and three-dimensional band gaps in the radiofrequency range, then to investigate how the specific features of these *hypersonic phononic crystals*, as an increasing part of the community dubbed them, could lead to a significant enough conceptual and technological breakthrough making it possible to reach performance far beyond that of the highly robust, firmly established high-frequency SAW and bulk acoustic wave (BAW) devices. Once this objective is established, works were undertaken both to investigate elastic wave propagation features at a fundamental level in such hypersonic crystals and to propose structures mimicking the operation of conventional radiofrequency devices used in RF electronics or in photonics, with the open goal to develop the field of *phononics*. Over time, this hype faded somehow, until the idea of phononic structures spread through the micro-electromechanical systems (MEMS) community, which is now proposing more practical usages of the associated concepts as building blocks for their components. Following this resurgence, this field of higher-frequency phononics is reevaluated in the numerous disciplines of physics and engineering fundamentally concerned with controlling low-wavelength elastic waves, or even phonons, in any potentially vibrating structures. This encompasses NEMS, optomechanics, microfluidics, thermal transport, or even quantum information.

This chapter proposes to go through the rather brief history of hypersonic phononic crystals, emphasizing attempts to apply the related concept to radiofrequency applications. As a starting point, section 8.1 will highlight the characteristics of elastic waves propagating at frequencies in the GHz range and account how these distinctive features have contributed to their undeniable success in wireless telecommunication applications. Then, section 8.2 will discuss the peculiarities of the fabrication of micron-sized structures and will shed light on the technological breakthroughs, which have been necessary to realize the first hypersonic phononic crystals. Elaborating on the specificities of these hypersonic crystals, section 8.3 will present early works taking inspiration from photonics or from the microwave world and will discuss why a direct transposition of these concepts to elastic wave RF components does not prove profitable. In contrast, section 8.4 will present examples of adoption of phononic crystals by the MEMS or the photonics community, where these structures bring an added value compared to

more established building blocks. Finally, a short conclusion will discuss the perspectives towards potentially interesting applications of hypersonic metamaterials.

8.1. Hypersonic elastic waves and their applications

Hypersound, sometimes also termed *microsound*, can be defined as elastic waves propagating at frequencies ranging from a few hundreds of MHz up to a few tens of GHz, although a definite agreement on the exact frequency limits of this rather recently introduced regime is yet to be reached. In this frequency range, propagation of acoustic waves in fluids, such as water or air, over significant distances (i.e. more than several micrometers) becomes difficult due to viscous losses. Hypersonic wave propagation is therefore usually restricted to solid media or to very confined microfluidic cavities. Typical wavelengths are then in the range of a few tens of micrometers down to some hundreds of nanometers. At this scale, material defects such as grain boundaries, dislocations or even interface roughness remain usually small enough to prevent the scattering or diffusion phenomena encountered for thermal phonons at THz frequencies. Hypersonic waves can thus propagate over fairly large distances, and their mathematical and physical description remains within the frame of the classical theory of elastic wave propagation in solids [CUF 12], meaning that interactions with the quasi-particles of the propagating medium can be neglected.

As shown in Figure 8.1, the frequency range for hypersound coincides with the part of the electromagnetic spectrum used for most radio transmissions. Operation of these systems in the MHz to GHz range is motivated by the fact that electromagnetic waves exhibit rather long propagation distances in free air (up to a few kilometers) at these frequencies, as the absorption by gases in the atmosphere remains relatively low. While the lower end of the spectrum, in the 100–400 MHz range, is mostly used for broadcasting signals such as frequency modulated (FM) radio or television signals, the 400 MHz–3.5 GHz range is now almost fully exploited for mobile communication systems, with some specific applications such as military, sensor systems or even microwave ovens interspersed in between the allocated frequency regions. In this range, radio signal carrier frequencies are high enough to ensure that relative bandwidths remain large enough to offer wireless communication systems satisfying data rates.

If electromagnetic (EM) waves are obviously unmatched as an information carrier, then the basic law stating that the characteristic dimension of a filter is comparable to the carrier wavelength prohibits the integration of EM filters in hand-held devices. As hypersonic waves exhibit wavelengths smaller by a factor of 10^5 than electromagnetic waves with the same frequencies, it has early been suggested that a significant size reduction could be achieved for some signal processing functions by manipulating elastic waves in solids instead of

electromagnetic waves. From the 1970s to the 1990s, a large host of surface acoustic wave components such as resonators, filters, delay lines and identification tags were first demonstrated and then came into mass production to propose miniaturized analog electronic signal processing devices. Nowadays, most of these components have been replaced by numerical data processing systems, due to progress in high-speed computing circuits. Yet, the sensitivity requirements of the current telecommunication standards impose being able to sample high-frequency signals with enough resolution to be able to detect a weak useful signal received from a base station positioned kilometers away from the receiver while not being disturbed by strong interferers, which may be located in close proximity to the mobile phone. This operation can certainly be achieved by numerical signal processing, at the expense, however, of electrical power consumption. Such a trade-off is clearly not acceptable for implementation in mobile handsets, and radio signals are therefore still processed by analog circuits, which filter the RF signal before amplifying, and frequency down-converts it before digitizing. Modern data transmission circuits hence remain dependent on analog band-pass filters made of miniature acoustic resonators, and their number is even increasing as the radiofrequency spectrum becomes increasingly fragmented. Options such as carrier aggregation (splitting the RF signal bandwidth over several carrier frequencies for a more efficient usage of the fragmented spectrum) or multiple-in-multiple-out (MIMO) antennas capable of performing electromagnetic beam-forming (enabling spatial filtering and therefore allowing simultaneous usage of the same portion of the spectrum by multiple users at different positions with respect to the same base station), which will both be deployed in the fifth generation of mobile communications and will even require a further increase in the number of acoustic components in a radiofrequency front-end [YOL 17].

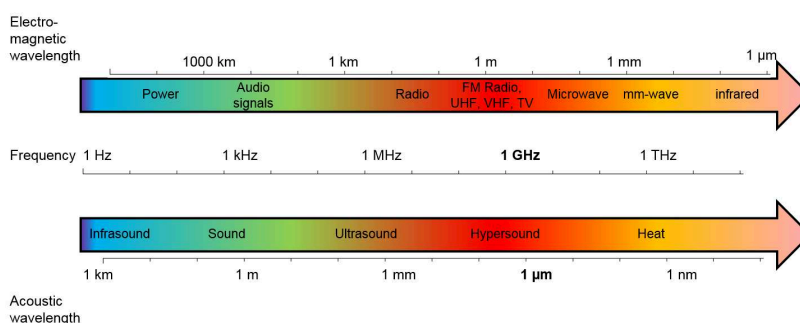


Figure 8.1. Domains for acoustic wave and electromagnetic waves and comparison of their respective frequency and wavelength scales. For a color version of this figure, see www.iste.co.uk/romero/metamaterials.zip

Replacing the propagation of electromagnetic waves by elastic waves however requires an efficient way to transduce an electrical signal into acoustic waves and vice versa. Perhaps the most efficient, and, incidentally, the first transduction mechanism historically used is piezoelectricity: a voltage carrying a signal can be transformed into strain exhibiting the same time dependence through the converse piezoelectric effect; this produces an elastic wave that propagates in the piezoelectric material and gets manipulated by the geometrical features of the device. The generated wave usually propagates up to a set of receiving electrodes where the stress fields generated by the wave cause, due to the direct piezoelectric effect, the appearance of time-varying electrical charges, that is, of a current transporting the processed signal. Electrostatic, electrostrictive or magnetostrictive transduction mechanisms are sometimes also used, but these are usually weaker effects and require bias voltages or magnetic fields to operate, while piezoelectric devices remain fully passive. The simplest application of this concept is a delay line, illustrated in Figure 8.2: two bulk acoustic wave transducers made of zinc oxide (ZnO) piezoelectric films sandwiched between two electrodes are used, respectively, to launch and detect elastic waves. In between, the propagation medium is a sapphire rod (Al_2O_3) whose function is only to allow for a propagation distance long enough to delay the transmitted signal compared to a direct transmission of an electric signal. Most delay lines used in signal processing circuits, such as early radar systems or even analog television receivers, make however use of surface acoustic waves (SAWs). SAWs correspond to vibrations guided along the surface of a semi-infinite substrate with an amplitude decaying exponentially away from the surface. Depending on the considered propagating half-space, waves with different characteristics (velocities, polarizations, etc.) can be encountered. Rayleigh waves are probably the most well-known form of surface waves. These sagittally polarized, dispersion-less and theoretically loss-less waves (provided, of course that the substrate itself does not exhibit significant intrinsic losses or structural defects) have been in use since the 1960s. The main advantage of surface waves is their intrinsic sensitivity to whatever occurs at the surface of the substrate. This basically means that it is possible to access and control directly the wave propagation path using planar structures. A key element in the development of SAW devices is the invention of the so-called *interdigitated transducer* (IDT) by White and Voltmer in 1965 [WHI 65] and their association with high-quality mono-crystalline bulk substrates that allowed easily generating and using cheap lithography techniques inherited from the microelectronics industry, which will be described in further detail in section 8.2.1. Interdigital transducers consist of a periodical arrangement of metal electrodes alternately connected to two bus bars used to convey an electrical potential. A basic surface-wave delay line is illustrated in Figure 8.2(b).

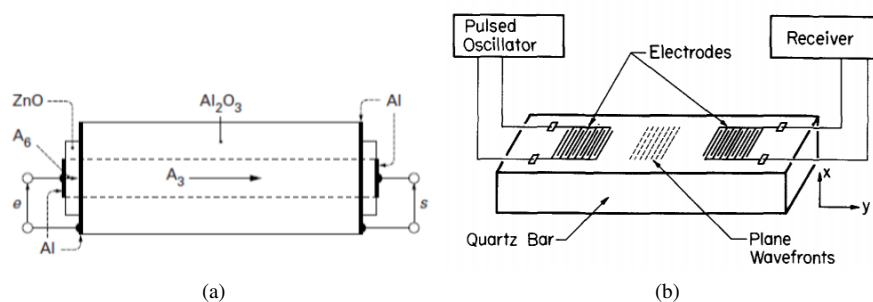


Figure 8.2. Example of delay lines: (a) bulk acoustic wave delay line (from [DIE 01]) and (b) surface acoustic wave delay line (from [WHI 65])

For a given material, elastic wave propagation mode and structure, we define an *electromechanical coupling factor*, which corresponds to the ratio of power transferred from one domain (electrical or mechanical) to the other during one wave period. At most, this coefficient can reach 90% in high-performance piezoelectric ceramics [YAM 08]. Material losses of such ceramics are however prohibitive when operating at frequencies higher than a few MHz, hence preventing their use in RF communication devices. Single-crystal materials, such as quartz, lithium niobate or lithium tantalate, are a more well-suited alternative. In principle, electromechanical coupling factors of the order of 50% can be reached for lithium niobate or lithium tantalate, but the combination of substrate orientation and propagation mode suited for practical applications usually limits the coupling factors to below 10% [DEF 01]. This means that only a similar fraction of the signal can be efficiently processed and transformed back at the output of the signal processing component, leading to components exhibiting insertion losses in excess of 20 dB. Such a situation can no more be tolerated as modern telecommunication systems require very weak signals to be processed with minimal attenuation (current filters used in the mobile phone industry require 1 dB loss only, 2 dB maximum). To overcome the limitation imposed by the relatively small electromechanical coupling factor, structures have been made resonant: since only a fraction of the power can be transduced during one wave period, power is accumulated over many periods up to the point of equilibrating the power inputs with losses within the resonant structure. In the case of surface waves, resonators can be obtained by encompassing an interdigital transducer in between two reflectors, simply built by depositing another periodical array of metal strips, usually referred to as *reflective grating*, as shown in Figure 8.3(a). Efficient reflection occurs when the pitch of the grating equals half the wavelength, that is, at the Bragg condition. The reflection coefficient per strip is however quite low (usually in the range of 1–4%), as reflection occurs because of the association of a strong modulation of the electrical boundary conditions with a weak perturbation of the mechanical conditions. Thus, SAW reflectors are usually made of close to 100

short-circuited electrodes. In the case of BAW resonators, relying on a thickness mode resonance, the most simple structure (although when it comes to microfabrication, things get more complex) is to form a freestanding membrane of piezoelectric material, since the air/solid interface provides a nearly perfect reflector. Hence, such a structure, shown in Figure 8.3(b), is now referred to as a *film bulk acoustic resonator* (FBAR). Due to structural strength concerns, an alternative structure relying on positioning the piezoelectric film atop an acoustic one-dimensional Bragg mirror, as sketched in Figure 8.3(c), is also industrially employed, and is referred to as *solidly mounted resonator* (SMR). Despite continuous work on more exotic structures, the industrial landscape for RF elastic wave devices is now almost fully filled with these SAW or BAW resonators only, and this situation has settled to this state since the early 2000s, with only incremental improvement since then.

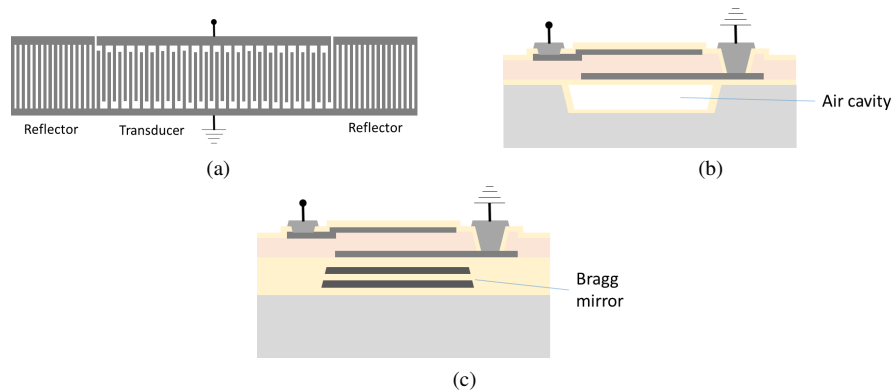


Figure 8.3. Main resonator types used in the RF filter industry: (a) SAW resonator, (b) FBAR and (c) SMR.

8.2. Hypersonic crystals

When the first experimental demonstrations of the occurrence of phononic band gaps were reported in the late 1990s for audible frequencies, it became quite clear that the concept could be applied to perform advanced signal processing. The first articles reported in the literature obviously dealt with structures operating in the sonic or ultrasonic regime because of their relative ease of fabrication, hence echoing the early days of photonic crystals in the microwave regime. As stated in the introduction, the so-called hypersonic regime refers to operating frequencies in the range of 100 MHz to a few GHz. In solids, this leads to characteristic dimensions of the order of the micrometer. The transposition of the phononic crystal concept to higher frequencies, where applications are potentially numerous, then has to overcome technological issues inherent to patterning at the micron scale. In addition, practical implementation

calls for compact and efficient devices, ideally based on the preferred solution for the realization of acoustic-based RF wireless devices, that is, exploiting the piezoelectric effect observable in well-chosen substrate. A typical hypersonic crystal could therefore be:

- a micron-scale device;
- an electromechanical device, with an electrical to mechanical transduction (and conversely) ideally induced by piezoelectricity;
- a device able to perform a specific function (a resonator, a band-pass filter, etc.);
- a device that could be fabricated using large-scale processes.

In summary, an RF phononic device is a micro-electromechanical system (MEMS).

The most natural way to produce phononic crystals in this length scale is therefore to rely on classical cleanroom technologies, as is the case for conventional RF electro-acoustic devices. The difficulties that are to be faced are then similar: as a general rule, MEMS design is as strongly driven by the functions and operations it should fulfill as it is by the constraints and tolerances imposed by the manufacturing process.

In this section, we will briefly introduce some typical microfabrication techniques that have proved relevant for phononic crystal fabrication. We will then find how a hypersonic crystal design can be tied to the associated technological constraints. The last part of this section will then give practical examples reported in the literature of phononic crystals exhibiting frequency band gaps in the sub-GHz to GHz frequency range.

8.2.1. Micron-scale fabrication

8.2.1.1. A short note on MEMS fabrication processes

MEMS technology directly derives from the technological processes developed for the microelectronics industry. Yet, where integrated circuits (IC) are essentially planar devices making use of a limited number of materials, MEMS devices usually make use of whatever materials and geometries required to achieve the desired functionality. This leads to what can be considered as a major strength, as well as one of the main complications of the MEMS technology: the possibility to put together a variety of processes and materials to create very versatile devices exhibiting a potentially rich physics, at the expense, however, of a certain amount of predictability in the fabrication process and on the device operation. It could be said that the main key for a successful manufacturing of an MEMS device lies in an awareness of what can be achieved in the context of a robust and repeatable process to find the better

trade-off between ideal design and actual fabrication, including the inevitable uncertainties related to some material properties.

There exists a very wide variety of microfabrication processes. This chapter does not aim to cover them in detail, and specific resources will fulfill this function in a much better and more exhaustive manner: there are no standard fabrication for MEMS devices, and this assertion is all the more true in the case of phononic crystals, as phononic devices are at a very early stage. Still, we will try here to give a rough idea of some of the technologies that may be involved.

As we mentioned earlier in this chapter, the MEMS technology finds its roots in the planar processes used in the microelectronics industry. Here as well, as for integrated circuits, the idea is to find simple, large-scale fabrication processes for devices with features that are bound to get ever tinier. A MEMS fabrication process can be described as the implementation of a sequence of basic steps, combined and potentially repeated many times over a substrate.

The substrate is ideally a commercial wafer, that is, a thin, polished slice of a specific material with a diameter of a few inches, up to 400 mm, for the currently most advanced nanoelectronics fabrication lines. The most conventional wafer dimensions are 300 mm for nanoelectronics, 200 mm for power electronics or silicon MEMS and 100 mm for more exotic substrate materials (typically the piezoelectric materials used in the SAW industry), with a recent trend for the latter to increase diameters towards 150 mm. Silicon obviously dominates the MEMS technological world, a significant number of reliable processes having been developed over the years on this semiconducting substrate in the context of microelectronics. Yet, it is not the preferred material for electro-acoustic devices that require piezoelectricity. In the surface acoustic wave industry, monocrystalline piezoelectric substrates such as quartz, lithium niobate or lithium tantalate dominate the market. Single-crystal materials are usually grown from an ultrapure material source through the so-called Czochralski method, although other efficient means of artificial synthesis have been developed over the years. Quartz, for instance, is grown using hydrothermal methods proposed in 1905 that have been gradually improved over the years, allowing the synthesis and mass production of artificial crystals exhibiting the same properties as natural crystals as early as in the 1970s. These processes lead to *boules* that are subsequently sliced along desired, precisely defined crystal orientations and then surface-polished.

A MEMS fabrication process involves two main process families. The first relates to the so-called *front-end*, that is, to cleanroom-related process steps; the second to the *back-end*, that is, to the packaging of the fabricated device.

The key aspect of the front-end fabrication flow lies in the possibility to transfer a desired pattern onto this substrate at the micron scale. This pattern transfer may occur

directly, by direct milling of the substrate, but as a much more general rule, pattern transfer is achieved indirectly by means of *surrogate layers* that can be easily shaped and subsequently removed (in other words, sacrificed) after transferring the pattern onto the wafer.

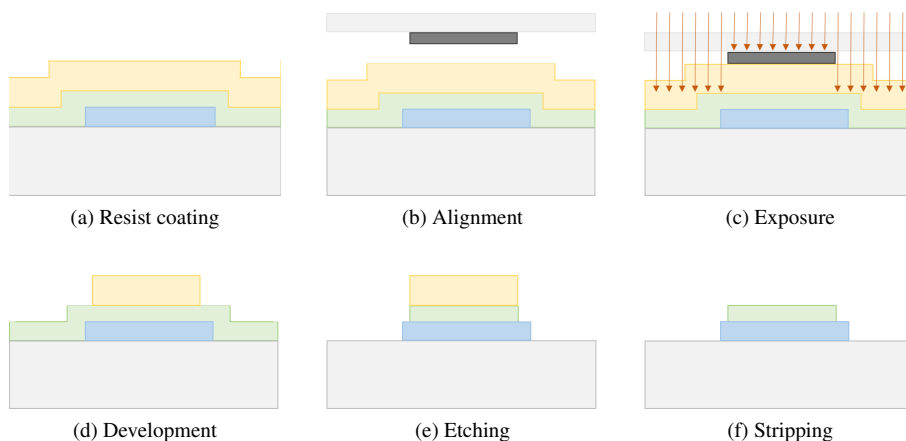


Figure 8.4. Generic process sequence for photolithography. For a color version of this figure, see www.iste.co.uk/romero/metamaterials.zip

Lithography is the generic process used to shape such surrogate layers. This process is a direct inheritance of the techniques used in the printing industry in the 19th Century. In the MEMS fabrication process, its principle is to apply the following steps to a substrate, illustrated in Figure 8.4:

1) *Resist coating*: the substrate is coated with a polymer film, called a *resist*. This coating is made thin (100 nm–10 μm) and highly uniform by spreading it over the whole sample area by centrifugation. Variations of these techniques involve spraying a mist of photoresist over the wafer, which is particularly efficient to obtain a coating made of a particularly low-viscosity photoresist (technique known as *spray coating*); dipping the substrate in a highly viscous photoresist, therefore leaving usually a thick coating (technique known as *dip coating*) or finally laminating a solid polymer film over the substrate. This last technique is particularly useful when the wafer already contains mobile microstructures that could be destroyed by the surface tension forces brought by any liquid coming in contact with them. After coating, the photoresist is left drying for a few minutes on a hot plate to evaporate excess solvents and leave an almost solid film.

2) *Alignment*: the coated substrate is then aligned with the so-called *photomask*, which is usually a translucent quartz (or some low-thermal-expansion glass) plate covered by a thin sheet of chromium patterned in the shape of the structure we want

to transfer to the substrate (or sometimes in the shape of the inverse image of these structures). The substrate is positioned under the mask, so that mask patterns, which will be ultimately photolithographically reproduced, are aligned over already existing structures on the substrate: the first pattern transferred to a wafer usually includes a set of alignment marks that is used as a reference for subsequent process steps. The most advanced lithography tools benefit from automated alignment, which relies on machine pattern recognition and offer positioning precisions (*registrations*) typically in the 100–300 nm range.

3) *Exposure*: the substrate and the mask are then irradiated. In contact lithography, the photomask is put in direct contact with the wafer using a *contact aligner*. This is a rather inexpensive and very mature technology that allows reaching resolution below 1 μm , well within the requirements of most MEMS fabrication processes, but clearly below the requirements of modern SAW devices. The industrial alternative is then to use *projection lithography*, more precisely *stepper lithography* that presents the advantage of reducing mask wear by avoiding direct contact with the substrate and that allows, in the case of stepper lithography, us to reduce the projected mask pattern using a highly complex high-resolution lens system, hence allowing us to both reduce the constraints on mask fabrication and reach much higher resolution (down to 250 nm). In all cases, the chromium patterns shadow the UV irradiation, while in non-protected areas, the irradiation triggers chemical reactions in the resist that locally change its chemical properties. The simplest irradiation source is a light bulb, although ultraviolet (UV) light is preferred for its shorter wavelength and therefore smaller diffraction limit. Advanced lithography relies on deep-ultraviolet (deep-UV) light sources. As an alternative for very-high-resolution features, we can mention the possibility to use electron-beam lithography, based on electron irradiation of an appropriate resist. This last technique is mask-less, with a highly focused electron beam (down to nanometer size) being moved across the sample and alternatively switched on or off to directly draw patterns without the need to supply a mask. The drawback is the long time needed to perform a high-resolution scan over a full wafer, compared to an illumination of the whole area at once. Therefore, it is only employed for the most size-critical process steps, such as drawing nanometer-size transistor gates in advanced nanoelectronics.

4) *Development*: the substrate is then bathed in a chemical solution capable of dissolving the resist that has been chemically modified during the previous exposure step. This leaves the non-irradiated areas unaffected, causing a transfer of the chromium patterns on the photoresist film. The photoresist is then chemically stabilized by a second baking at a larger temperature than the drying step.

5) *Pattern transfer*: the pattern hosted by the photoresist is then transferred on the wafer, for example, by etching. The substrate is subjected to a chemical or physical process capable of etching the material exposed at the surface of the substrate, in the regions not protected by the photoresist patterns. This process may be a dissolution of the material by a chemical reaction occurring in liquid phase (so-called *wet etching*) or

sometimes in gaseous phase. Common techniques involve also some ion bombardment (gathered under the term *dry etching*), where the kinetic energy of accelerated ions is used to eject matter from the surface. Ion etching techniques are often assisted by some chemical reactions occurring on the surface between highly reactive ionized species formed in the plasma and the materials located on the substrate. This technique is therefore known as *reactive ion etching*. In both cases, the photoresist can act as a protection for parts of the substrate, so that patterns that were located on the mask are ultimately transferred on the substrate.

6) *Stripping*: after etching, the photoresist patterns are removed by a chemical dissolution of the polymer, leaving a substrate ready for restarting the next photolithography cycle.

The cumulation of material deposition steps, lithography and etching, makes up close to 90% of a MEMS integration process. Performing them in sequence can produce relatively complex three-dimensional structures while using mostly planar techniques. The strength of these techniques is that they are applied on a full substrate at a time, while the objects fabricated can be extremely small, so that a large number of them can be fabricated collectively. Hence, cleanroom processes are referred to as *very-large-scale integration* (VLSI). As an illustration, BAW filters occupy typically an area smaller than 1 mm^2 while fabricated on 200 mm diameter silicon substrates. Hence, a single fabrication sequence can simultaneously produce more than 25,000 individual components per wafer.

8.2.1.2. *Design rules*

Despite their versatility, cleanroom fabrication processes do not allow every geometry to be produced. Therefore, the design of micron-sized structures such as phononic crystals has to always respect *design rules*, which dictate what can be fabricated and often impose limitations to the type of structures we would like to fabricate.

Design rules for micron-scale phononic structures, such as holey phononic crystals, originate from the two fabrication process conditions we covered in the previous section:

1) photolithography processes, as precise as they may have become when one considers large-scale integration of nanoelectronic circuits, always face a resolution limit. Even though the latest equipment are nowadays capable of generating nanometer-scale features using electronic beam writing or deep-UV immersion scanners, such tools cannot (yet) be considered as mainstream for phononic applications, as their cost remains prohibitive for anything else than advanced microelectronics, not to talk about academic laboratories. Therefore, it is more reasonable considering working with somehow less expensive equipment, which offer resolutions dictated by the diffraction limit of UV or deep-UV, that is, in the range

of 250 nm in the most favorable case. Additionally, the selectivity of the etching processes, that is, the ratio between the removal rate of the material we want to etch and the removal rate of the photoresist mask, requires that, in order to form features with thicknesses or depth in the micron range, a photoresist coating of the same order of magnitude becomes necessary. Generally, the ultimate resolution that can be achieved with a photoresist mask is roughly in the same range as the photoresist thickness. This means that phononic crystal geometries have to exhibit smallest dimensions in the range of 1–2 μm : this smallest dimension has to apply to individual scatterers or to the spacing between them.

2) etching processes provide smooth and vertical sidewalls in only a few very specific cases: silicon or silicon dioxide. When considering the patterning of piezoelectric materials, such as lithium niobate or aluminum nitride, reactive ion etching usually leaves sidewalls in the range of 80 degrees, as shown in Figure 8.5(a), sometimes even less. Small-diameter holes may therefore be limited in depth, as they form a cone that would close before reaching the desired depth. This usually adds additional constraints on the depth that can be achieved.

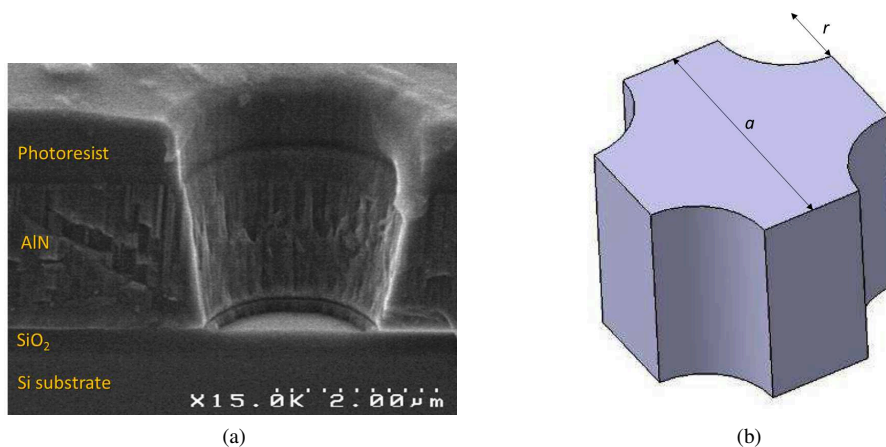


Figure 8.5. Illustration of a phononic crystal made of an array of holes embedded in a solid matrix: (a) limitation in sidewall angle revealed by a scanning electron microscope image of an actual hole obtained after etching holes in an AlN film and (b) indications of critical process dimensions.

Given the fact that the opening of phononic band gaps usually requires relatively large filling fractions (see Chapters ??), the limiting factor is usually the spacing AQ1 between two neighboring scatterers, which must remain large enough to comply with design rules. Translated in terms of dimensions for the example of a square lattice made of holes etched in a solid matrix, shown in Figure 8.5(b), photolithography

processes impose minimum values to the radius r of holes and to the spacing $a - 2r$ between neighboring holes. For this reason, phononic band gaps are usually limited to frequencies below 1 GHz. Switching to higher-order band gaps may be a solution to move towards higher frequencies, but at the expense of relative width.

8.2.2. Experimental demonstrations of hypersonic band gaps

Despite the technological difficulty to fabricate phononic crystals exhibiting large band gaps at GHz frequencies, several demonstrations have been successfully achieved. Following some early works on the characterization of one-dimensional structures such as semiconductor superlattices or one-dimensional phononic structures [BAR 98, DHA 00, OZG 01], the true starting point for two-dimensional phononic structures is the work of Gorishnyy *et al.* in 2005 [GOR 05]. For the first time, a periodic structure made of a triangular lattice of holes with a filling ratio of up to 39% directly formed in photoresist coated on glass was fabricated and its band diagram was experimentally determined by Brillouin light spectroscopy. This evidenced branches in the 2 GHz region, as well as folding of modes at the edge of the Brillouin zone.

Subsequently to this experiment, demonstrations of phononic crystals compatible with the major types of elastic wave resonators have been proposed. In section 8.2.2.1, we will describe phononic crystals fabricated on bulk monocrystalline substrates and compatible with surface acoustic waves devices. Then, we will detail in section 8.2.2.2 crystals realized on freestanding membranes, the so-called *phononic crystal slabs*, which are compatible with many MEMS processes and especially with Lamb wave resonators, a kind of resonator that has still to find an industrial application, but which is extensively studied in the academic world. Finally, section 8.2.2.3 will focus on the few examples of phononic crystals for bulk waves and discuss the difficulty related with integrating a phononic crystal suitable for a BAW device.

8.2.2.1. Phononic crystals for surface acoustic waves

The combination of surface acoustic waves and piezoelectric monocrystalline solids such as quartz, lithium tantalate (LiTaO_3) or lithium niobate (LiNbO_3), among others, occupies a prominent position in the field of wireless telecommunications and signal processing. Monocrystalline substrates indeed offer piezoelectric and electromechanical coupling properties that remain unmatched by the currently available piezoelectric thin films. The theoretical demonstration by Wu *et al.* of the capability of a two-dimensional phononic crystal to open band gaps for surface acoustic waves [WU 05a] offered therefore particularly rich applicative prospects while constituting a very good field for more fundamental investigations.

The very appealing properties of monocrystalline substrates are however most of the time counter-balanced by the difficulty of processing these materials, which are

quite often complex oxides, using standard micromachining technologies. Fabrication then stands as a challenge, while design is not made easier: the strong anisotropy of acoustic wave propagation inherent to piezoelectric materials, combined with the quasi-systematic mixing of shear and longitudinal polarizations, puts tighter constraints on the geometrical parameters of the periodical structure itself [WU 04, LAU 05].

The first experimental demonstration of complete band gaps for surface acoustic waves propagating on lithium niobate substrates was performed by Benchabane *et al.* [BEN 06]. The phononic crystal consisted of a square array of $9\ \mu\text{m}$ diameter air holes with a period of $10\ \mu\text{m}$. With such dimensions, the band gap extended from 203 to 226 MHz. Its existence has been characterized in transmission by using sets of interdigitated transducers (IDT) in delay line configuration. Two sets of delay lines were measured: a set of classical lines, acting as reference to calibrate the limited electric transmission of the setup, and a set of lines in which the phononic crystal was inserted, as shown in Figure 8.6. The comparison of the measured transmission (defined as the ratio between the output power measured on the receiving IDT and the incident electrical power applied to the emitting IDT) in Figure 8.6(b) for the reference (dashed) and for the delay lines with the crystal (thick continuous lines) reveals that in the low-frequency side, the crystal does not strongly perturb the transmission. Within the band gap, marked as the gray region, the transmission between the two transducers drops considerably, proving its existence. This experiment paved the way for a fully electrical characterization of high-frequency phononic crystals, and its scheme remained for long a reference setup reused in further studies.

The most conventional fabrication technique for the etching of the array of holes in lithium niobate is reactive ion etching, using sulfur hexafluoride (SF_6) as the gas providing reactive species (F^- ions) [BEN 06]. Due to the high chemical stability of lithium niobate and the non-volatility at process temperature of some of the reaction's by-products (LiF in particular), the etching process has to operate mostly in a ballistic regime where material removal is achieved through the transfer of kinetic energy to the surface of the sample rather than through chemical reactions. Hence, the pressure in the etching chamber had to be kept relatively low (about $2\ \mu\text{bar}$) and the RF power used to excite the plasma had to be set to a relatively high value (200 W) to provide more kinetic energy to ions bombarding the surface. Even in such conditions, the etch rate was only $50\ \text{nm}/\text{min}$ (as a comparison, silicon etch rates can be as high as $50\ \mu\text{m}/\text{min}$). This meant that several hours were necessary to etch holes $10\ \mu\text{m}$ deep. Photoresist masks are not capable of withstanding such long exposure to a high-energy ion bombardment. Therefore, the etching process had to be made more complex, by using a $1\ \mu\text{m}$ electroplated nickel mask. However, even in such conditions, the holes obtained proved conical rather than cylindrical, with a sidewall slope of about 17% for $10\ \mu\text{m}$ diameter holes, as visible in the inset of Figure 8.6(a).

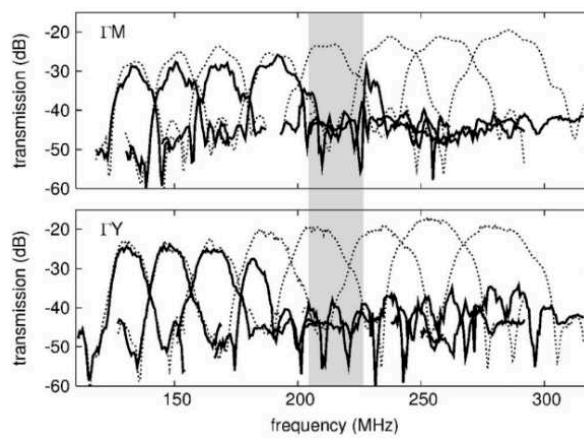
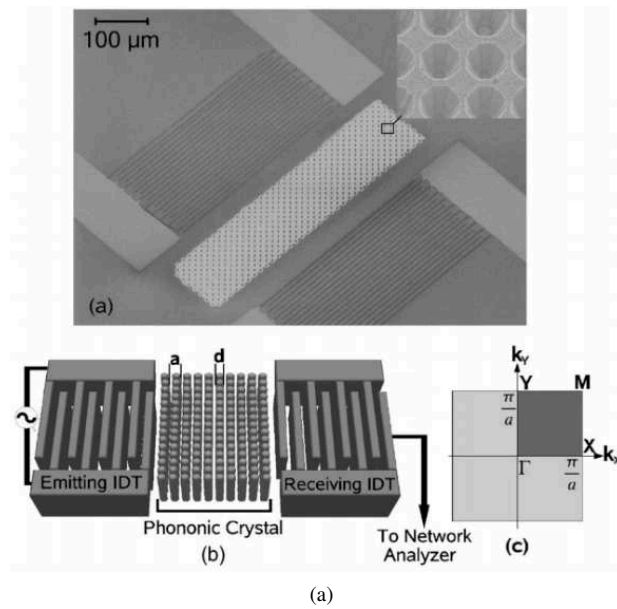


Figure 8.6. Surface acoustic wave delay line for probing a phononic crystal made of square lattice of holes in lithium niobate: (a) scanning electron microscopy image of the fabricated device and sketch of the experimental setup and (b) electrical measurements of several delay lines (solid: including the phononic crystal; dashed: without phononic crystal) to cover the frequency range surrounding the band gap (in gray) [BEN 06]

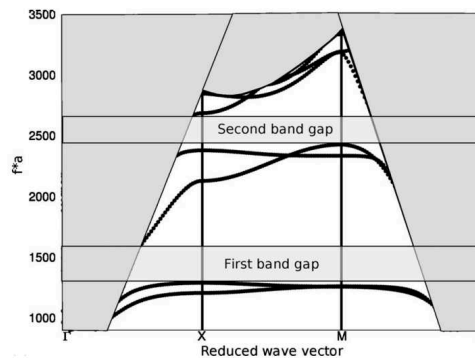
Several other techniques were tried to improve the etching process, especially electron irradiation in [ASS 08]. The principle consists in writing patterns using an electron beam as in e-beam lithography, but this time without photoresist. Instead, the electronic charges accumulated on the surface force a local inversion of the ferroelectric domains in lithium niobate and make the material sensitive to chemical etching by pure hydrofluoric (HF) acid. The process durations proved, however, to be similar to reactive ion etching, and the holes proved also conical, with a sidewall slope of 12%. Finally, the shape of the scatterers seemed to be difficult to control, as electrostatic forces tend to spread the electrons apart from each other at the surface of the insulating lithium niobate.

Due to the difficulty to etch holes in monocrystalline piezoelectric materials, work has been also devoted to form phononic crystals for surface acoustic waves on silicon substrates, in order to benefit for the easier processing of this material, which is the reference substrate for microfabrication. Wu *et al.* proposed to excite surface waves on silicon substrates using a thin film of piezoelectric zinc oxide (ZnO) deposited on top of a silicon substrate and positioned at the level of the emission and reception transducers [WU 05b]. Using a technique known as deep reactive ion etching, particularly efficient to etch high-aspect-ratio holes in silicon substrates, they managed to form a phononic crystal with holes 80 μm deep for a diameter of only 3.5 μm . This paper proposed also an improvement of the measurement setup: in [BEN 06], eight delay lines with different IDT periods were needed in order to cover the full phononic band gap as well as frequencies in its vicinity, as shown in Figure 8.6(b). The transducers used in [WU 05b] were slanted in order to simultaneously excite several wavelengths and therefore to directly cover a wide frequency range with a single delay line, although it resulted in a decrease in the overall electrical transmission.

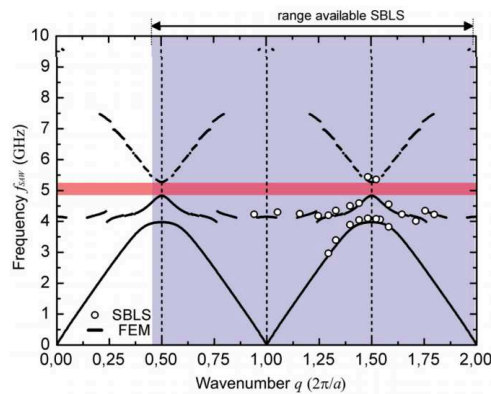
One particular feature of the interaction of a surface wave with a phononic crystal is visible in Figure 8.6(b): after the band gap, the transmission of acoustic waves is not necessarily recovered. For a phononic crystal made of holes periodically arranged in a piezoelectric substrate, optical heterodyne interferometry reveals a strong scattering of the surface wave as the crystal acts as a diffraction grating [KOK 07]. The strongest contribution to the attenuation, however, occurs when the surface wave dispersion crosses the so-called *sound line*, that is, becomes faster than the slowest bulk wave and is therefore no more guided at the surface. It is also supposed that the finite depth and the conic shape of the holes enhances the coupling to bulk waves.

Aside from phononic crystals exhibiting band gaps arising from Bragg scattering, resonant metamaterials in which local resonances open hypersonic band gaps have been more recently investigated [LIU 14]. For guided waves, this idea can be seen as an extension to sub-wavelength scatterers of the well-known principle of mass loading, which consists in affecting the relation dispersion of surface elastic waves by creating corrugations or by manufacturing high-aspect-ratio structures on the surface of the

substrate hosting the propagation [MAY 91, SOC 12], with the aim, in particular, to slow down the propagation. It has, for example, been shown that phononic crystals of thick metal pillars deposited on a homogeneous surface could exhibit hybridization gaps caused by local resonances of the pillars in addition to the Bragg band gaps caused by the periodicity of the array [KHE 10a, ACH 11, YUD 16]. Interestingly, this ensures a way to open a band gap, or several, below the sound line, as shown in Figure 8.7(a). A first experimental demonstration in the GHz frequency range used aluminum pillars formed on a silicon substrate [GRA 12]. With 100 nm thick pillars having a radius of 95 nm, disposed in a square array of 500 nm period, the band structure has been determined by surface Brillouin light scattering and evidenced band gaps around 5 GHz, as shown in Figure 8.7(b).



(a)



(b)

Figure 8.7. Band gap for surface acoustic waves obtained through the coupling with local resonances of pillars: (a) theoretical calculation [KHE 10a] and (b) experimental measurement using surface Brillouin light scattering [GRA 12]

Local resonances have also been used to investigate contact resonance effects in granular materials [BOE 13, HIR 16, ELI 16], for instance, in the case of micron-sized polystyrene spheres adhered to a substrate, and are shown in Figure 8.8(a). These last experiments, performed through optical excitation and interferometric optical measurements, allowed us to determine the attenuation of surface acoustic waves propagating in a glass substrate as a function of frequency and proved the existence of an attenuation peak at the resonance frequency of the Hertzian contact, as shown in Figure 8.8(b).

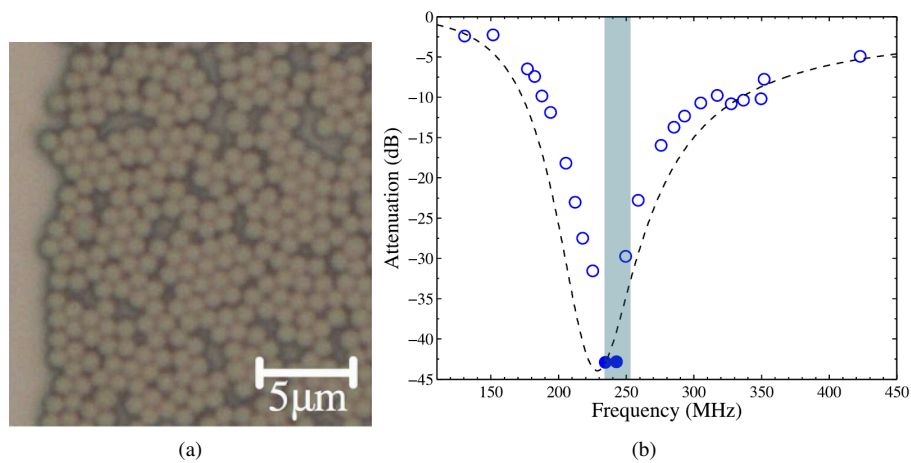


Figure 8.8. Resonant metamaterial for surface acoustic waves made of polystyrene micro-spheres adhered on a glass substrate: (a) optical micrograph and (b) measurement of the attenuation for Rayleigh waves propagating through a 170 μm strip of micro-spheres [ELI 16]

Despite the possibility of relying on resonant band gaps, of effectively designing Bragg band gaps lying below the sound line [YUD 12] or of annular patterns supporting local resonances to reduce coupling to other modes [ASH 17], some authors considered that surface acoustic wave phononic crystals lacked vertical confinement. They proposed therefore to switch to thin plates offering a vertical confinement preventing radiation in a substrate. Such crystals inserted in a vertically limited medium were soon called *phononic crystal slabs*.

8.2.2.2. Phononic crystal slabs

Propagation of waves in slabs calls for the study of phononic crystals for plate waves. As early as 2006, that is immediately after the theoretical demonstration of the existence of phononic crystals exhibiting stop bands for surface waves, Hsu *et al.*

calculated the dispersion curves for Lamb waves propagating in thin plates containing a periodic array of cylindrical inclusions [HSU 06, HSU 07b]. They demonstrated that the consideration of traction-free surfaces delimiting the slab significantly modifies the band structures compared to a bulk crystal, as they derive from the dispersion curves for Lamb of plate waves. Nevertheless, they demonstrated that band gaps can still be obtained, for relatively large filling fractions.

First experimental demonstrations of phononic crystal for plate waves have been performed the same year by two independent groups. Hsiao *et al.* considered a slab made of epoxy encompassing steel spheres disposed in a square lattice [HSI 07]. With the spheres having 4 mm diameter, a complete phononic band gap opened around 300 kHz. Acoustic waves were excited using an emission transducer and were coupled to the slab by a prism, while an interferometric measurement scheme was employed. Closer to the hypersonic range, Olsson *et al.* [OLS 07] fabricated a micron-sized crystal made of a square lattice of cylindrical tungsten (W) scatterers (lattice parameter: 45 μm ; radius, 14.4 μm) embedded in a silicon dioxide membrane (4 μm thick). This combination of materials has been chosen for compatibility with the industrial fabrication of the interconnects in integrated circuits. As for SAW phononic crystals, a completely integrated measurement setup was fabricated along with the crystal: transmission of Lamb waves through the crystal was measured by a delay line made of an aluminum nitride (AlN) transducer formed on top of the silicon dioxide membrane, as shown in Figure 8.9(a). Electrical measurements, reproduced in Figure 8.9(b), reveal in this case a stop band ranging from 59 to 76 MHz.

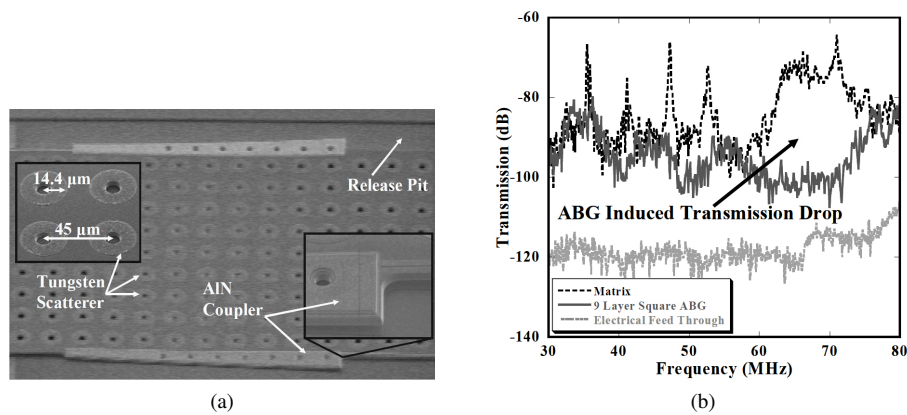


Figure 8.9. Phononic crystal for Lamb waves: (a) scanning electron microscopy (SEM) image of the crystal made of tungsten scatterers embedded in a silicon dioxide membrane inserted between two AlN transducers and (b) electrical measurements of the transmission, revealing a band gap ranging from 59 to 76 MHz [OLS 07]

Following this first demonstration, other groups proposed different combinations of materials and crystal structures to increase the band gap center frequency and its width, the goal being ultimately to reach frequencies used for telecommunication applications (400–3,500 MHz). Mohammadi *et al.* obtained an attenuation band ranging from 119 to 150 MHz (i.e. a 23% relative bandwidth) using a crystal made of cylindrical holes disposed as an hexagonal lattice (lattice parameter, 15 μm ; radius, 6.4 μm) on a 15 μm thick silicon membrane [MOH 08]. Here, the reduction in lattice parameter is responsible for the higher-frequency range, while the move to an hexagonal lattice and the increase of the filling fraction of the scatterers promote a wider stop band. Soliman *et al.* managed to obtain a significant attenuation of the acoustic transmission between 1 and 1.8 GHz by realizing a crystal with even more aggressive dimensions: 0.65 μm diameter tungsten scatterers were disposed in a square lattice with a 2.5 μm period inside a 1.15 μm thick silicon membrane [SOL 10b].

An alternative approach is to embed the phononic crystal in a material exhibiting a large sound velocity, such as aluminum nitride (AlN). This material being also piezoelectric, the phononic crystal can be integrated directly along transducers, in a way similar to earlier works on surface waves. With a phononic crystal slab realized in a silicon dioxide/aluminum nitride membrane, Gorisse *et al.* demonstrated an attenuation band for Lamb waves ranging from 600 to 950 MHz [GOR 11] using a square array of almost cylindrical holes. Simultaneously, Kuo *et al.* obtained an attenuation band for Lamb waves ranging from 850 MHz to 1.2 GHz, using a square array of “X”-shaped holes (lattice parameter, 5 μm ; thickness, 1 μm ; $4.2 \times 0.75 \mu\text{m}$ arms) formed also in an AlN membrane [KUO 11].

As for surface acoustic waves, locally resonant phononic crystals were also proposed, relying on pillar structures formed at the surface of a plate to open a band gap [HSU 07a]. First works considering “thin” plates (with respect to the wavelength) demonstrated that the local resonances of the pillars interact with the modes of the plate, which manifests by the opening of band gaps [PEN 08]. Thin circular plates periodically disposed within the main, thicker, plate, shown in Figure 8.10, were also proposed and exhibited a slow mode corresponding to the flexural mode of individual thin plates [SUN 10]. In both cases, this usually opens a stop band at a frequency below the Bragg band gap, although the band gap location is essentially conditioned by the resonant frequency of the scatterers. Hence, such structures are not directly suited for obtaining band gaps at frequencies compatible with RF applications.

A particularity of phononic slabs is that they are realized on elastic plate, which supports the propagation of a host of modes: symmetric and antisymmetric Lamb waves as well as shear horizontal plate waves. This produces a much more complex band structure than three-dimensional phononic crystals or than phononic crystals for surface waves. For this reason, the interaction of a phononic crystal with transducers

is more complex than in the case of phononic crystals for surface waves. This is, for example, illustrated in Figure 8.11(a), which shows the measured electrical transmission of a Lamb wave delay line used to probe a phononic crystal. A significant transmission attenuation is visible between 600 and 900 MHz, while the theoretical band gap is only expected to extend from 776 to 828 MHz [GOR 11]. Clearly, in the process of converting the Lamb waves into Bloch modes of the crystal and conversely at the output of the crystal, a large part of the acoustic power generated by the emitter transducer is lost. While this is expected inside the band gap, as only evanescent Bloch modes may transfer power through the crystal, it is fairly unexpected outside of the stop band. A first explanation for this is that the AlN or ZnO transducers used to excite or to detect waves are only capable of exciting symmetrical Lamb waves. As such, Bloch modes with shear horizontal polarization, identified in Figure 8.11(b) (left), are not expected to be excited [SOL 10b, KUO 11]. Additionally, even some Bloch modes with out-of-plane transverse or with longitudinal polarization may not be excited if their mode shape is orthogonal to the polarization of the incident or transmitted Lamb waves [GOR 11]. Such modes are then called “deaf bands” [HSI 07]. Finally, some flat bands, such as the ones labeled “b” and “c” in Figure 8.11(a), may be so localized that they do not generate strong peaks in transmission spectra. This extended attenuation range compared to the sheer phononic band gap proves highly beneficial in most applications, where phononic crystals are expected to act as reflectors. Hence, phononic crystal slabs faced more interest than phononic crystals for surface waves and were rapidly adopted by the MEMS community as will become evident in section 8.3.2.

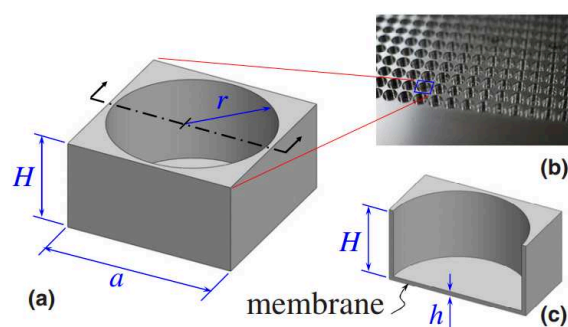
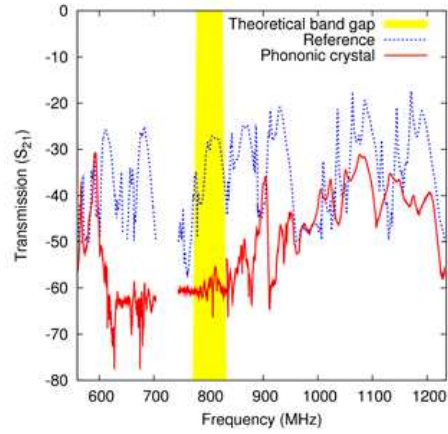
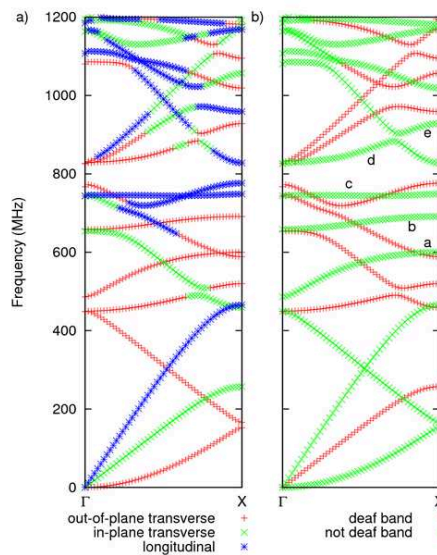


Figure 8.10. Square lattice phononic crystal plate made of periodic membranes: (a) schematic of the unit cell, (b) photograph of the fabricated sample and (c) cross-section of the unit cell [SUN 10]



(a)



(b)

Figure 8.11. *SiO₂/AlN-based phononic crystal slab [GOR 11]: (a) electrical transmission of a set of Lamb wave delay lines with (continuous red curve) or without (blue dashed lines) phononic crystal inserted between transducers. The theoretical band gap position is highlighted in yellow. (b) Band structure for the phononic crystal: (left) determination of the polarization of Bloch modes and (right) identification of deaf bands. For a color version of this figure, see www.iste.co.uk/romero/metamaterials.zip*

8.2.2.3. *Phononic crystals for bulk acoustic waves*

Despite extensive work on phononic crystals for surface acoustic wave or plate waves, no notable reports of phononic crystals that could benefit bulk acoustic wave resonators have been published, although this technology is now the second standard for elastic wave RF components behind SAW filters, and is certainly more mature than the field of Lamb wave devices.

In the field of bulk acoustic wave devices, Bragg mirrors have been proposed as early as 1965 [NEW 65] to isolate the piezoelectric resonant cavity from its surroundings. With the advent of thin-film bulk acoustic resonators, this idea has been extensively developed in the solidly mounted resonator (SMR) technology. Mirrors used nowadays in this technology differ from simple quarter-wavelength stack of materials. They are usually optimized to provide a stop band for all vertically propagating wave polarizations, in order to reduce any possible leakage of acoustic power out of the resonant cavity, even the marginal-thickness shear waves generated by mode conversions during reflection of the main thickness-extensional mode at the edges of the resonator electrodes [MAR 05]. Even though they are designed only for vertically propagating waves, they prove also efficient for waves propagating in the lateral direction, which usually act as parasitic modes for bulk wave resonators [TAL 06]. They have therefore even been proposed to provide a vertical confinement for waves guided in a piezoelectric film [KHE 08, KON 10, TAK 16], as will be more detailed in section 8.4.2. Such one-dimensional structures are however not considered as being phononic crystals or elastic metamaterials.

Phononic crystals capable of opening a band gap at the frequencies where bulk waves are exploited could hold the promise of extreme three-dimensional confinement of waves in BAW resonators and therefore boost quality factors beyond their actual levels. However, opening a band gap at their frequencies of operation, that is, between 1.5 and 3.5 GHz, proves difficult: as discussed in sections 8.2.1.2 and 8.2.2.2, micro-fabrication techniques allow the formation of phononic crystals with band gaps reaching frequencies up to 1 GHz. More aggressive dimensions could theoretically increase the range of frequencies achievable, by increasing the frequencies at which the Bragg condition related to the spacial periodicity of the phononic crystal, or the Mie scattering related to the dimensions of the scatterers, occurs [OLS 09]. As an example, phononic crystals made of cylindrical holes disposed in a square lattice within a silicon matrix were studied in [OSE 18]. A lattice parameter of 940 nm and a filling fraction of 76% are necessary to open a band gap extending between 2 and 3 GHz. Such a high filling fraction reveals critical to decrease the frequency of the band gap from several GHz down to 2 GHz. It provides however almost unrealistic spacing between adjacent holes (15 nm) and is therefore impossible to implement in practical applications.

One of the only effective structures reported to date relied on an industrial process for integrated circuit manufacturing [BAR 15]: a phononic crystal was realized using the metal interconnects between transistors, made of 165 nm copper stripes separated by 85 nm, embedded in a low-permittivity solid dielectric (SiOCH) material. Due to the high miniaturization, the calculation of the band structure, shown in Figure 8.12(b), reveals the opening of a band gap extending from 2.54 to 6.35 GHz. Obtaining such fine dimensions has been, however, only made possible by the huge research and engineering efforts that the nanoelectronics industry deployed over decades to continuously keep the pace on miniaturization of integrated circuits imposed by Moore's law. Therefore, the patterning of these materials is well established and optimized to form sub-micron features. Forming sub-micron size piezoelectric structures, which would be mandatory for collocating a high-frequency hypersonic crystal with a bulk wave resonator, still remains an extremely challenging task as was discussed earlier in section 8.2.1.2.

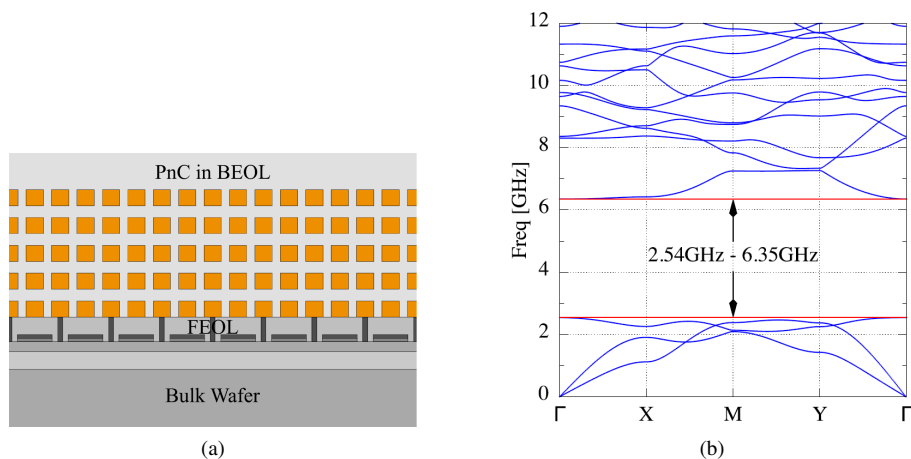


Figure 8.12. Phononic crystal made of CMOS interconnects [BAR 15]: (a) schematic of the structure and (b) calculated band structure. For a color version of this figure, see www.iste.co.uk/romero/metamaterials.zip

A second issue is that the stack of materials (piezoelectric film, electrodes, passivation, Bragg mirror layers, etc.) of BAW resonators is already optimized for the main functionality of the filter. Therefore, phononic crystals have to be tailored for

such a complex set of materials and have to offer wave confinement without affecting in any other mean the stringent performances of the device. As a result, hypersonic crystals suitable for bulk wave applications is still an open investigation topic.

8.3. Phononics for RF signal processing

After early works aimed to demonstrate the ability to push phononic crystals to the hypersonic range and to overcome microfabrication challenges related to their actual implementation, at least for surface or plate waves, research groups have started focusing on applications that could benefit from this new concept.

The major characteristic of phononic crystals is their ability to open a phononic band gap, which forbids the propagation of acoustic waves regardless of their direction. This called from the very early stages of research on this topic for envisioning a tight confinement of waves in geometrically defined structures. Taking inspiration from the microwave world and from photonics, researchers proposed two different classes of functions benefiting from this confinement: waveguides in which phononic crystal constrain waves to follow a very specific path, or resonant cavities, which are regions completely surrounded by a phononic crystal and therefore almost fully isolated from their surrounding.

8.3.1. Phononic waveguides

Any defect inserted in an otherwise perfect crystal adds a branch to the band structure. In particular, removing a full row of scatterers in a phononic crystal has the consequence of enabling a defect mode localized in the row. A slightly different view is to state that waves can be trapped in the defect row but cannot escape if their frequency falls within the band gap of the crystal surrounding the defect. This property is at the basis of light guidance in photonic crystals. Taking this inspiration, Kafesaki *et al.* [KAF 00] theoretically proved that defect modes obtained by removing a row of scatterers in a phononic crystal, illustrated in the example of Figure 8.13(c), can carry acoustic power through the crystal. Interestingly, near-perfect transmission is obtained in Figures 8.13(a) and 8.13(b), making the defect line act as an efficient waveguide. Unlike photonic waveguides, the defect modes may be of shear or longitudinal polarizations and may interact with each other, hence opening sub-band gaps, which may cause transmission drops in the waveguide at specific frequencies within the guiding band gap. Such a mechanism is

not only tied to conventional phononic crystals, but has been also theoretically demonstrated in a locally resonant phononic plate [OUD 10]. That case is particularly interesting as, since local resonances may open a band gap at frequencies lower than the Bragg regime, the waveguide may remain single mode even in the case of relatively large guides, for example, obtained by removing three lines of local resonators, as shown in Figure 8.14.

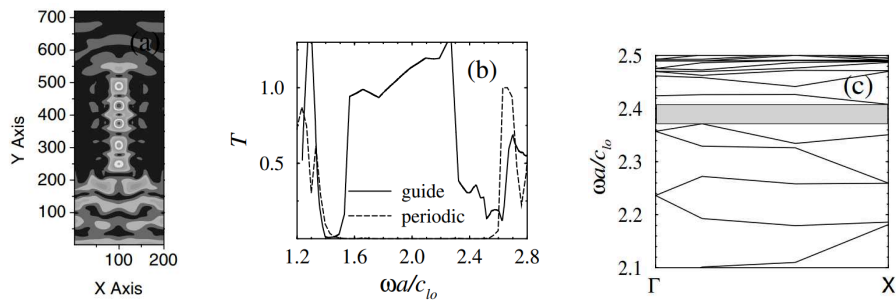


Figure 8.13. Phononic crystal waveguide [KAF 00]: (a) example of the calculated acoustic field amplitude of a defect mode established in a missing row of cylinders in a square lattice, (b) comparison of the transmission coefficient as a function of frequency for elastic wave propagating in a defectless crystal (dashed line) or through a line defect and (c) the band diagram calculated for a supercell made of 5×5 array of scatterers, including the defect line

Slightly later, Khelif *et al.* [KHE 02] took this time analogy from microwave transmission lines. The addition of lateral branches, called *stubs*, to a main transmission line causes interferences between the main wave propagating in the transmission line and the wave that has propagated into the stub and has been reflected by the end of this usually short line. Hence, depending on the length of the stub, this forces locally a node or an antinode, which generates features in the transmission spectrum such as transmission zeros at specific frequencies. This can be thought as the hypersonic equivalent of a Helmholtz resonator for audible sound. A similar behavior was theoretically demonstrated in [KHE 02] for a stubbed phononic waveguide in the case of a scalar wave propagating in water with a crystal consisting of periodical solid scatterers. Figure 8.15(a) shows how an acoustic wave reflects from the end of the stub and interacts destructively with the incoming wave field. It was especially shown that the length or the width of the stub significantly affects the

number and frequency of transmission zeros, as evidenced in Figure 8.15(b), which shows a transmission spectrum calculated for stubs having different widths.

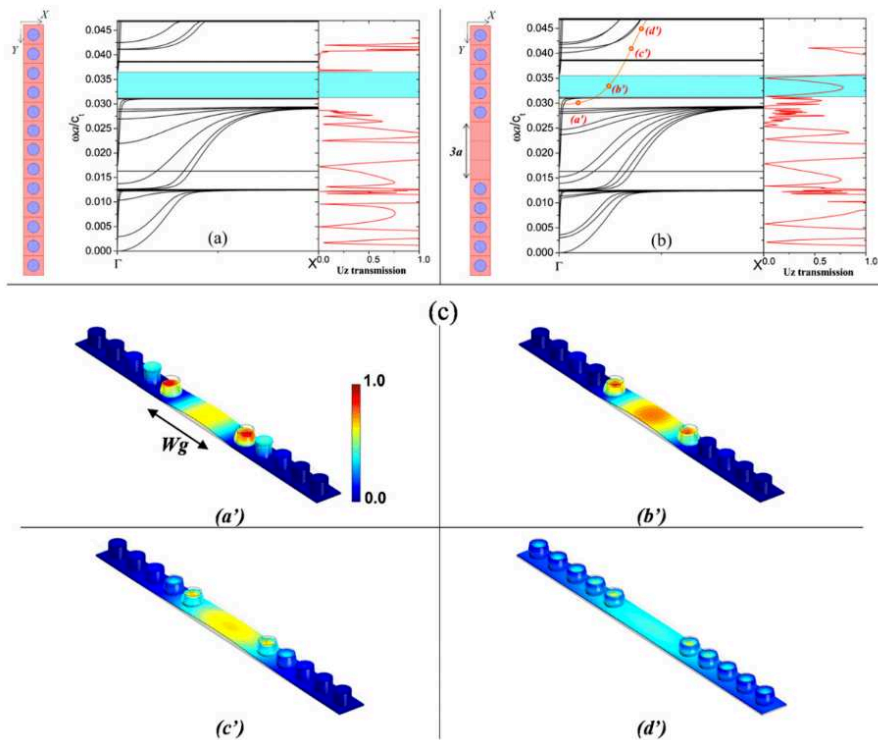


Figure 8.14. Waveguide formed in a resonant phononic crystal slab [OUD 10]: (a) band structure and transmission coefficient of a supercell made of 13 rubber pillars on an epoxy plate. (b) Band structure of a supercell representing the waveguide structure obtained by removing three pillars from the previous structure. (c) Displacement amplitude of the defect mode plotted for different wavenumbers, at positions indicated by red cycles in (b). For a color version of this figure, see www.iste.co.uk/romero/metamaterials.zip

Further expansions of these concepts were investigated, this time also experimentally, to propose more complex functions. For example, Pennec *et al.* [PEN 05] used two cavities, formed by the removal of a scatterer in the phononic crystal, to couple together two waveguides, as sketched in Figure 8.16. The coupling was facilitated by stubs extending out of the waveguides towards the cavities. At the resonance of the cavity mode, waves propagating through one of the guides could be

redirected towards the second waveguide, hence promoting a demultiplexing function.

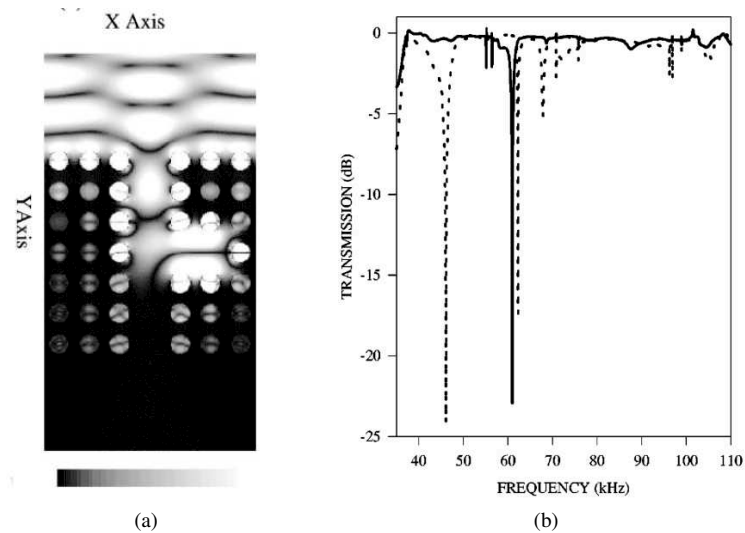


Figure 8.15. *Stubbed phononic crystal waveguide [KHE 02]: (a) calculated field amplitude at the frequency at which the stub causes a transmission zero and (b) calculated transmission coefficient as a function of frequency for a stub width of one (solid line) or two (dashed line) unit cells*

Guidance by a line defect waveguide was experimentally demonstrated in 2004 [KHE 04], by forming a waveguide by removing rods from a periodic two-dimensional lattice of steel cylinders immersed in water. In this series of experiments, it was proved that the complete band gap is capable of forcing waves to travel across sharp bends. In 2007, Hsiao *et al.* focused on a solid phononic crystal slab [HSI 07]. They fabricated a phononic crystal structure made of steel spheres embedded in an epoxy matrix, already mentioned in section 8.2.2.2. Interferometric measurements of the wave amplitude revealed an attenuation of approximately -45 dB for the wave transmitted through the six-period-long waveguide, which has to be compared with an attenuation of about -60 dB for the phononic crystal itself, and about -30 dB for the epoxy slab alone. These values proved to be strongly frequency-dependent and not uniform in the frequency range of the phononic band gap due to the complex band structure of the waveguide. Additionally, the additional 15 dB attenuation compared to the sole epoxy medium was too high for practical applications. As such loss rates were not observed in early experiments in water, they are likely to originate from coupling losses at the entrance or the exit of the

waveguide, where mode conversions exist between the Lamb or plate waves of the slab and the modes of the crystal or conversely, as well as from intrinsic losses of the defect modes themselves.

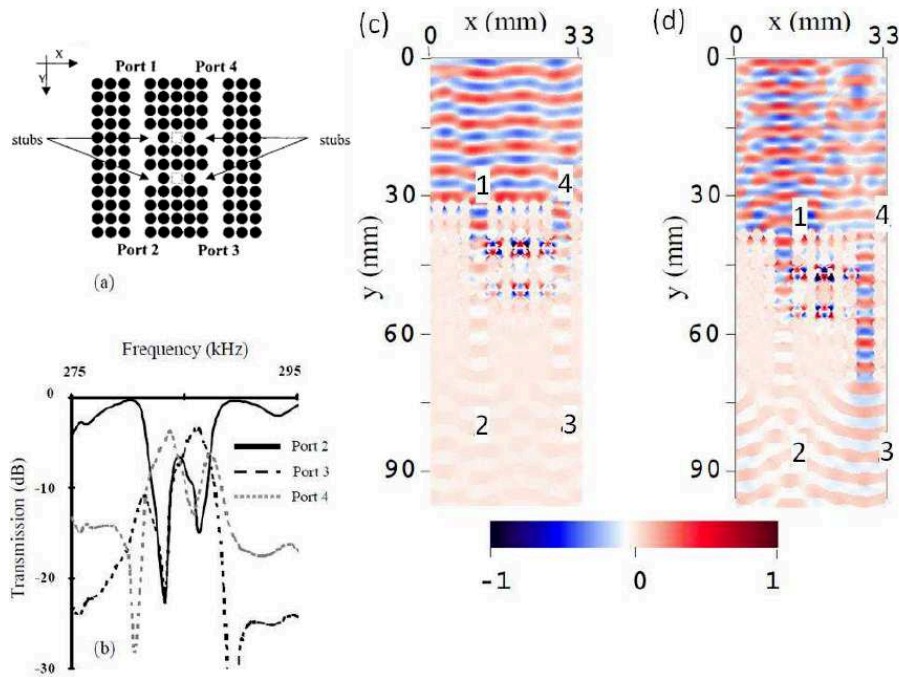


Figure 8.16. (a) Coupling between two stubbed waveguides through resonant cavities made of two vacancies in the phononic crystal. (b) Calculated transmission spectrum at ports 2, 3 and 4 for an input excitation at port 1. (c) Calculated fields at 283 kHz, corresponding to the frequency where the transmission drops at the level of ports 2 and 3, while it is enhanced at port 4. (d) Calculated fields at 286 kHz, where the transmission drops at ports 2 and 4, and is enhanced at port 3 [PEN 05]. For a color version of this figure, see www.iste.co.uk/romero/metamaterials.zip

All these demonstrations were performed in the 100–500 kHz range, therefore far below the radiofrequency range. Waveguiding of surface modes at a frequency close to 1 GHz was only demonstrated in 2015, by Benchabane *et al.* [BEN 15]. This demonstration required forming a square lattice (2.1 μm period) of holes (1.9 μm diameter, 2.5 μm deep) in a lithium niobate substrate, which opens a band gap ranging from 650 to 950 MHz. Surface waves were excited by chirped transducers capable of exciting waves from 630 to 1.3 GHz, which were fabricated by

electron-beam lithography to ensure a sufficiently fine resolution of the metal electrodes. Propagation of waves was imaged by scanning laser interferometry and revealed that a single-line defect effectively guides, within the band gap, waves in a micron-size guide. As for low-frequency experiments, an attenuation of 10 dB was measured between the entrance and the exit of the waveguide, also attributed to the modal mismatch between the incident and transmitted waves and the guided mode.

Despite an effective waveguiding behavior and the possibility to implement sharp bends, propagation losses exhibited by phononic waveguides remain too large for practical applications by at least an order of magnitude. Clearly, one of the main issues pertains to the matching of defect modes to the incident waves in order to transfer nearly all the power inside the guide. A second critical point is to reduce propagation losses in the waveguide itself. While these remain still open issues, the focus of the community has shifted towards another use of localized defect modes: resonant cavities.

8.3.2. Phononic crystal cavities

When defects consist in the removal of a single scatterer, or a group of scatterers, in a perfect phononic crystal exhibiting a complete band gap, they give rise to a highly localized mode and therefore to a strong confinement of waves inside and in the close vicinity of the defect. Khelif *et al.* investigated this experimentally, with an ultrasonic phononic crystal made of a square array of steel cylinders immersed in water [KHE 03]. They proved that the cavity formed by the removal of a single scatterer leads to the appearance of a sharp transmission peak within the phononic band gap otherwise characterized by a low-transmission (−20 dB) region, as shown in Figure 8.17(a). When several, reasonably spaced cavities are formed, mode splitting between the coupled cavities brings up several transmission peaks.

Eventually, they demonstrated that when a sufficient number of cavities are disposed in-line, the number of split modes becomes sufficient to form a transmission band contained inside the band gap. In Figure 8.17(b), this transmission band extends roughly from 275 to 305 kHz [KHE 03]. This provides another mechanism to implement a waveguide other than forming an extended line defect. In subsequent work, the same authors replaced cavities formed by the removal of a scatterer by inserting a line defect, that is, a spacing between two lines of unit cells of the crystal, in the direction perpendicular to the considered wave propagation direction [KHE 10b]. The band gap of the crystal ensures that waves are confined in this spacing and that the coupling between other line defects is evanescent. Such waveguides also exhibit a filtering behavior, since transmission through the set of resonators can only occur in the vicinity of the resonance frequency of individual cavities.

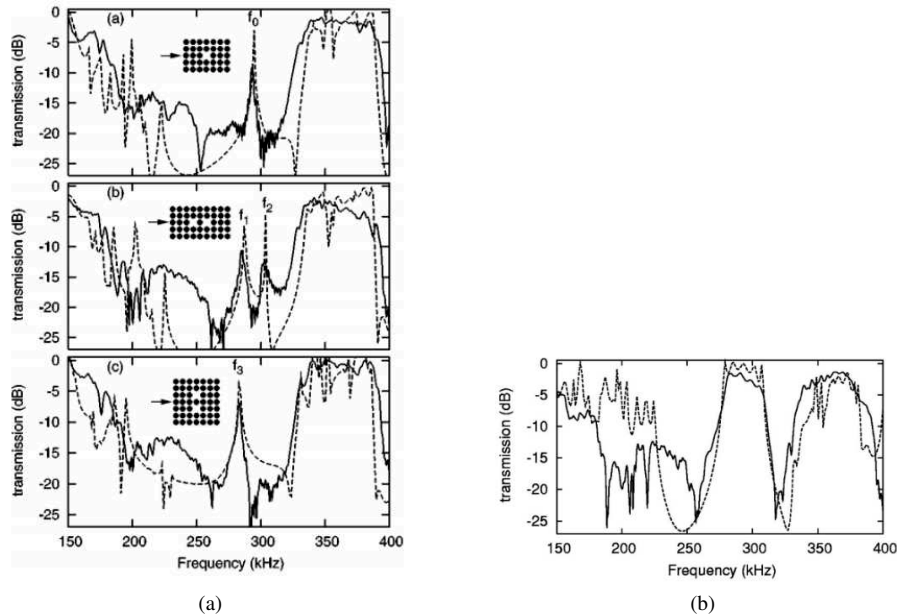


Figure 8.17. Transmission spectra for waves propagating in a steel/water phononic crystal in which several defects have been formed [KHE 03]: (a) single-defect cavities and couplings between two defects and (b) array of defects coupled to form a transmission band

Another type of resonant cavities is Fabry–Perot-like resonators, consisting in a free propagation path inserted in between two phononic crystals. Mohammadi *et al.* [MOH 09] introduced them in phononic crystal slabs. With the setup shown in Figure 8.18(a), they measured the transmission through the Fabry–Perot cavity and revealed the resonant modes they support. An example of such a measurement is shown in Figure 8.18(b). Sun *et al.* [SUN 09] demonstrated that the resonant modes of phononic crystal slab Fabry–Perot cavities are in fact conventional Lamb modes of the matrix slab. As they cannot couple to any mode in the phononic crystal in the frequency range of the phononic band gap, they are trapped in a resonant cavity, forming a resonance whose displacement amplitude and quality factor are only limited by the effective transmission coefficient of the phononic crystal and the quantity of power leakage out of the cavity they allow. As shown in Figure 8.18(b), Mohammadi *et al.* measured quality factors (defined as the ratio between the transmission peak center frequency and its -3 dB bandwidth) of 6,300 at a frequency of 126 MHz, with a phononic crystal extending over three periods [MOH 09]. This

may not seem an outstanding figure of merit for silicon micro-resonators, but could be certainly improved with longer phononic crystals providing better insulation. Experimental data provided in [MOH 09] reveal however that, although quality factors improve with the number of crystal periods, the transmission through the Fabry–Perot resonator decreases. This is indeed expected, as better isolation from the environment makes the probing of highly confined modes more difficult from an external source.

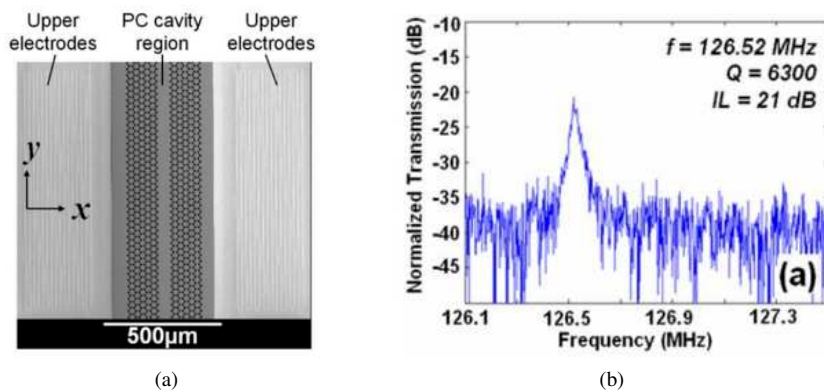


Figure 8.18. Phononic crystal slab Fabry–Perot resonators [MOH 09]:
 (a) scanning electron microscopy image of a Lamb-wave delay line used to characterize the resonant cavity and (b) electrical measurement of the fundamental cavity mode falling in the phononic band gap

To benefit from potentially high-quality factors while still being able to efficiently excite and detect the highly confined modes of Fabry–Perot cavities, Wu *et al.* proposed to directly insert the transducers inside the cavity. To demonstrate this idea, they inserted a ZnO/Si surface acoustic wave delay line inside a phononic Fabry–Perot cavity formed by etching a square array of cylindrical holes in the silicon substrate [WU 09], as sketched in Figure 8.19(a). In this configuration, instead of exciting propagating surface waves, the interdigitated transducer excites the low loss cavity modes, leading to a boost in the transmission coefficient of the delay lines by 7 dB, as revealed by Figure 8.19(b). Additionally, the phononic crystal provides a much more compact reflector than the conventional electrode gratings used in the surface wave filters industry. This comes, however, at the expense of parasitic dips visible in the electric transmission, caused by the multiple cavity modes, which are also excited by the interdigitated transducers.

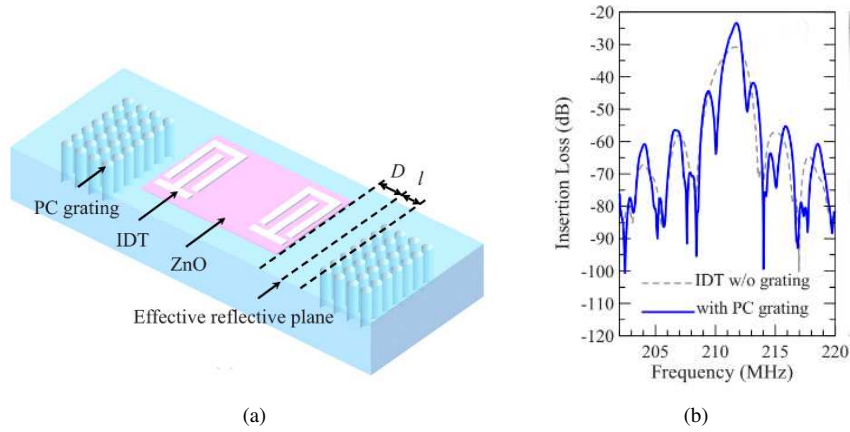


Figure 8.19. Insertion of transducers directly inside a Fabry–Perot cavity [WU 09]: (a) sketch of the resonator inserted in between two phononic crystals acting as reflector structures and (b) electric response of the resonator with the phononic crystal reflectors (solid line) or with conventional short-circuited electrode reflectors (dashed line). For a color version of this figure, see www.iste.co.uk/romero/metamaterials.zip

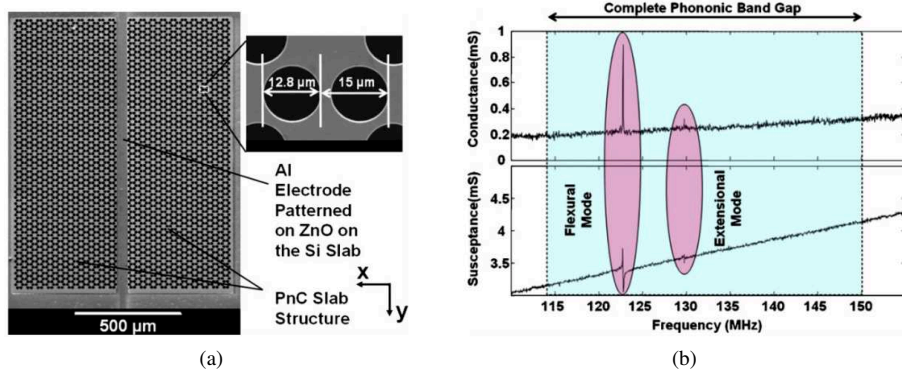


Figure 8.20. Phononic crystal employed as a reflector delimiting the resonant cavity of a Lamb wave resonator [MOH 11]: (a) scanning electron microscopy image of the fabricated device and (b) electrical measurement of the resonator response

Taking a similar scheme, Mohammadi *et al.* [MOH 11] inserted a single transducer inside a phononic crystal slab Fabry–Perot cavity, as shown in Figure 8.20(a), and obtained similar quality factors to their earlier experiments with transducers positioned outside of the cavity [MOH 09]. In the case of phononic

crystal slabs, the phononic crystal does not provide a better or more compact confinement to Lamb wave devices than the conventional membrane edges delimiting the resonant cavity employed in a majority of works, visible in Figure 8.21. It offers, however, a way of maintaining suspended membranes attached to the substrate by a support, which prevents the leakage of waves from the membrane to the surrounding medium, hence limiting anchor losses faced when employing solid tethers. This idea received a large interest from the MEMS community, and will be further developed in section 8.4.1.

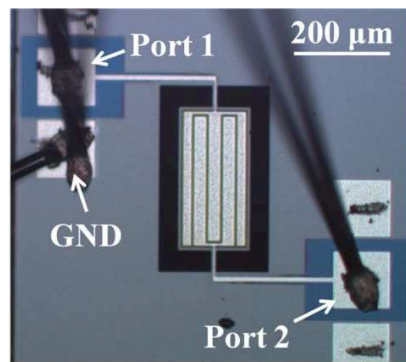


Figure 8.21. Conventional Lamb wave resonator with a resonant cavity delimited by a straight ending of the propagation medium

Before that, for the sake of completeness, we briefly describe similar attempts to replace the short-circuited electrode gratings conventionally used as reflectors for surface acoustic wave resonators by phononic crystals. These were reported after the first works on Lamb wave resonators. Liu *et al.* demonstrated a phononic crystal for Love waves guided in a silica film on top of a quartz substrate and used it as a reflector [LIU 14]. Their structure as well as an example of electric response are shown in Figure 8.22. The experimental quality factors were however almost one order of magnitude lower than what was obtained for Lamb wave resonators using phononic crystals as reflectors. A first explanation for this was the extremely high sensitivity of the quality factor to the positioning of the crystal with respect to the electrodes to ensure that electrodes are optimally positioned for the excitation of one specific mode of the relatively large cavity. The second point was the coupling of the Love waves with bulk waves of the substrate due to the finite depth of the holes used as scatterers. Elaborating on this, Wang *et al.* noted that such an effect occurs primarily when waves excited by the transducer impinge the phononic crystal: mode conversion between the Love wave (in their case, guided in a GaN layer on a sapphire substrate) and Bloch modes causes a significant excitation of bulk waves radiating in the substrate [WAN 15]. To overcome this fact, they implemented a

smooth transition between the free propagation medium and the phononic crystal, taking the form of a crystal starting with a gradient of scatterers diameter in the propagation direction. This way, they managed to obtain a quality factor of 880 for a resonator surrounded by a graded phononic crystal, compared to a quality factor of 248 for a sharp crystal. The drawback is, however, a loss in electromechanical coupling factor with the practical extension of the resonant cavity out of the transducer. This is due to the fact that transduction does not take place in the whole cavity, thus decreasing its efficiency. Additionally, even though this gradual matching of the crystal to the cavity improves quality factors, they still remain lower than what can be conventionally obtained using conventional short-circuited electrode reflectors. As for Lamb wave resonators, the benefit lies, however, in the reduced footprint offered by the very compact phononic crystal.

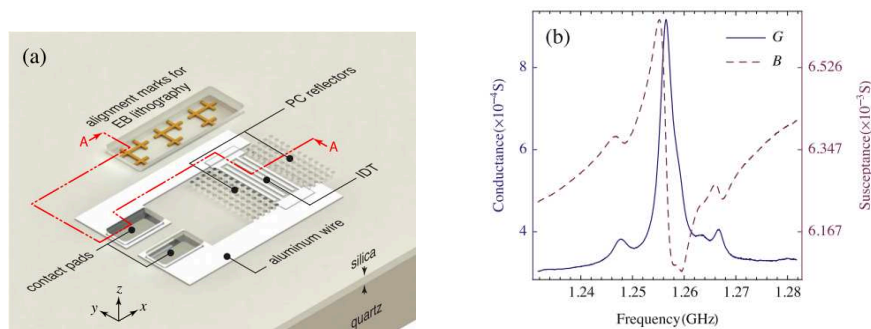


Figure 8.22. Love wave resonator using a phononic crystal as a reflector: (a) sketch of the resonator structure and (b) electrical response close to the resonance [LIU 14]. For a color version of this figure, see www.iste.co.uk/romero/metamaterials.zip

8.4. Practical applications of phononic crystals

Clearly, the initial expectations for phononic crystals in the 2000s, driven by the possibility to guide waves along phononic channels and to manipulate them using resonant cavities or stubs, are not living up to the expectations of the RF telecommunication systems community. Potentially practical implementations are mostly limited to their use as building blocks of resonator structures: mostly as very compact reflectors. Even so, their added value may be questioned, as well-established, simpler and at least effective reflector structures are already employed by the resonator community. Niche applications for phononic crystals however remain, notably in the field of MEMS resonators, SAW devices and in relation with photonics, which we detail in this section.

8.4.1. Phononics for MEMS resonators

As highlighted in section 8.3.2, phononic crystals do not perform more effectively than conventional reflector structures for acoustic resonators. This is especially true for Lamb wave (also referred to as contour mode) resonators that rely on ending abruptly the resonant cavity with a solid/air interface to implement a perfect reflector. Such resonators, implemented as suspended membranes, need however mechanical supports to remain attached to the substrate. These anchors may provide a path for acoustic leakage out of the resonators. This is where Sorenson *et al.* proposed to replace the usually straight tethers supporting the resonator body, an example of which is depicted in Figure 8.21, by a phononic crystal whose band gap falls around the resonance frequency of the resonator in order to confine acoustic waves in the resonant cavity. A first version of such a crystal is a line of ring-shaped resonant structures, an example of which is shown in Figure 8.23(a) [SOR 11]. With such anchors, the quality factor of the resonator considered in [QIN 16] increases from 2,660, in the case where straight tethers are employed, to 6,250. This comes, however, at the expense of adding small parasitic resonances at the edges of the phononic band gap. Using instead a gourd-shaped periodic structure, shown in Figure 8.24(a), which geometrically differs less from a conventional straight tether, Wu *et al.* obtained a reduced quality factor improvement (from 1,304 for a straight tether to 1,893 for the gourd-shaped phononic crystal tethered resonator, as visible in Figure 8.24(b)). They managed, however, to even remove some parasitic resonances that could be noted on measurements of resonators with straight tethers [WU 16].

For appropriate designs, the achievable quality factor increase can therefore be significant, and proves the effectiveness of phononic crystal tethers to suppress anchor losses. Yet, more conventional methods have already demonstrated a similar efficiency. The easiest and most straightforward method is to design straight tethers with a length corresponding to a quarter wavelength. Considering electrostatically actuated length extensional resonators, Jansen *et al.* have thoroughly investigated the dependence of the quality factor of the resonator on the length of the support tethers [JAN 11]. As shown in Figure 8.25, the quality factor of a suspended MEMS resonator can increase from 3,000 to 19,000 with a proper design of straight tethers, hence showing that there is no absolute need to involve more fragile and complex designs as phononic tethers.

Tu *et al.* have in addition demonstrated that periodic arrays of holes, although they efficiently decrease anchor losses, may increase the amount of thermoelastic damping by one order of magnitude [TU 12]. This is probably due to an increase in the coupling of shear deformations to compression of the matrix material. In the case of a Lamé mode resonator, this increased thermoelastic damping manages to replace anchor losses as the dominant loss mechanism.

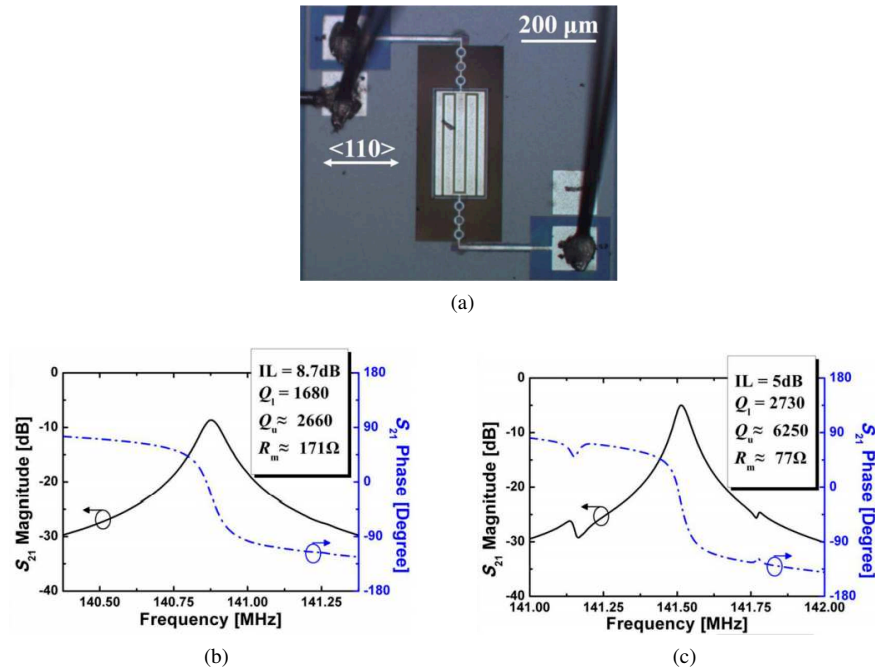


Figure 8.23. Lamb wave resonator with a phononic crystal tether based on a line of ring resonators (a) and measurement of a resonator with a conventional tether (shown in Figure 8.21) (b) or with a line of ring resonators (c) [QIN 16]. For a color version of this figure, see www.iste.co.uk/romero/metamaterials.zip

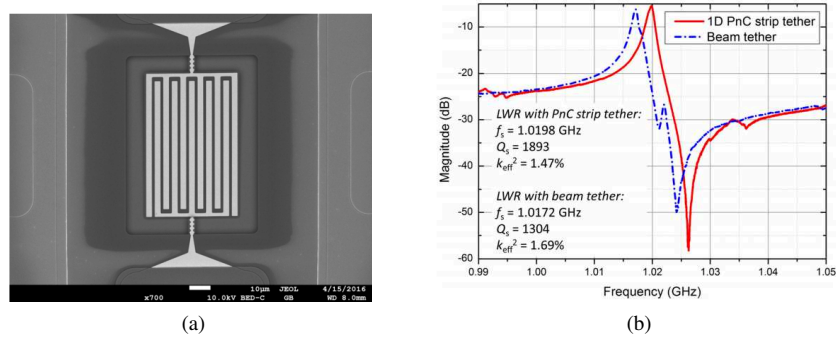


Figure 8.24. Lamb wave resonator with gourd-shaped phononic crystal tethers: (a) optical microscope picture; (b) measurement of a resonator (red continuous line) and comparison with a reference structure with a conventional tether (blue dashed line) [WU 16]. For a color version of this figure, see www.iste.co.uk/romero/metamaterials.zip

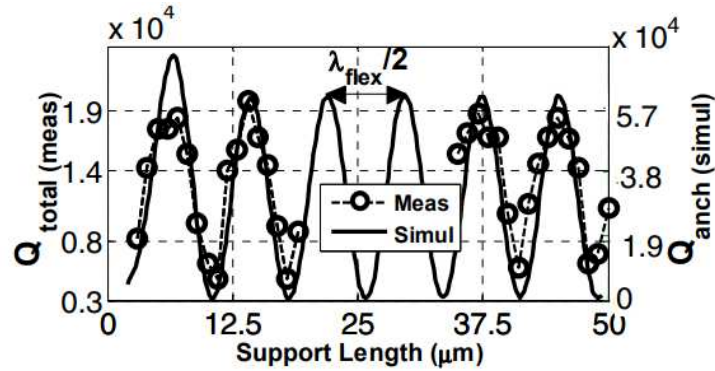


Figure 8.25. Dependence of the quality factor of a MEMS resonator on the length of its supporting tethers [JAN 11]

There is however one point for which phononic crystal anchors provide a clear added-value: heat dissipation. Campanella *et al.* have investigated the behavior of Lamb wave resonators whose resonant cavity is limited by a phononic crystal and compared it to that of a conventional resonator delimited by a solid/air interface. When applying relatively high electrical input power, the resonators delimited by a phononic crystal revealed lower temperature increase than conventional ones. Assuming that the phononic crystal does not impact the dependence of the resonance frequency on temperature (which is caused by thermal expansion of the whole structure, as well as by the dependence of the elastic constants on temperature) results in reduced frequency shifts due to temperature dependence of the resonance frequency [CAM 14] and therefore in a better frequency stability. This is very likely caused by the fact that the crystal, although filled with many holes, provides an additional path for heat dissipation compared to the abrupt ending of the resonator structure. The drawback is, however, reduced linearity, possibly attributed to the increased thermoelastic damping mentioned earlier.

As a conclusion, using phononic crystals as reflectors or as tethers for MEMS resonators is clearly not more effective than well-designed conventional tethers or air/solid interface reflectors. On the contrary, it may even increase the amount of thermoelastic damping compared to a fully solid structure. However, in some specific cases, it may provide a path for heat dissipation, which may find some interest if thermal stability is the major criterion sought. This is, however, not generally the case. Therefore, the interest of the MEMS community towards phononic crystals faded somehow with time.

8.4.2. Phononics for surface acoustic wave resonators

As we have seen in section 8.3.2, the initial attempts to replace the shorted electrode reflectors commonly employed in SAW resonators did not reveal a major gain in quality factors or in electromechanical coupling factors. Given also the fact, discussed in section 8.2.2.1, that fabricating these crystals in piezoelectric substrates drastically complicates the otherwise simple fabrication process for SAW devices, it seems very unlikely that this approach finds application in the SAW filter industry unless phononic crystals manage bringing about a genuine technological or conceptual breakthrough.

It cannot however be denied that the SAW industry nowadays faces technological challenges linked to the inevitable increase in the required operation frequency of filters. The major limitation in the operation frequency of SAW devices is the resolution of the interdigitated electrodes required to excite these waves, as the electrodes already exhibit submicron dimensions at frequencies higher than 1 GHz. This is a direct consequence from the relatively low propagation velocities of surface waves. Current standards at 2.45 GHz already call for finger dimensions lying straight at the limit of steppers used up to at least a few years back in the SAW industry, that is, 350 nm. The new resolution limit of 250 nm, set by more recent lower-cost projection lithography affordable by others than the IC industry, is about to be reached. Such dimensions moreover raise considerable reliability concerns, as the electric fields developing across sub-micron gaps reach rapidly extremely large values, which limits the power-handling capabilities of SAW devices. Therefore, the SAW filter community has been actively investigating other types of waves with higher phase velocities in the last four decades [HAG 72, TAN 07, CHI 10]. A solution is to deposit a thin piezoelectric film on top of a high-velocity substrate such as silicon, sapphire or diamond. In such structures, surface modes benefit from an increase in phase velocity due to the large stiffness of the substrate, seen through the evanescent tail of the mode. Truly guided modes, confined mostly in the piezoelectric film through total internal reflection, and exhibiting considerably large phase velocities, are often overlooked, as they usually suffer from lower electromechanical coupling factors.

Elaborating on this, Khelif *et al.* [KHE 08] proposed to completely guide waves in the piezoelectric film by relying on the confinement brought by an acoustic Bragg mirror. Taking the example of a tungsten/aluminum multilayer, they theoretically demonstrated that such a 1D phononic crystal can open an omnidirectional band gap and can therefore prohibit any radiation of waves towards the substrate in the frequency band of interest. Adding a piezoelectric film on top of the superlattice produces defect modes localized in the film, which acts as an effective waveguide. In such conditions, they proved that resonances can be obtained at 5.5 GHz for interdigitated electrode periods of 1.2 μm . Such a structure is reasonably achievable both in terms of electrodes dimensions and in the fabrication of the superlattice,

which only requires the deposition of six films on a substrate, a technological process that remains simpler than the processes in use by the RF BAW industry.

A similar idea was further considered by Koné *et al.* [KON 10], although their Bragg mirror did not necessarily open an omnidirectional band gap. Provided that the transmission of waves from the piezoelectric film to the substrate remains low enough (typically below -25 dB, as seen in Figure 8.26(a)) for waves mixing longitudinal and shear polarization at a wavelength compatible with the period of the interdigitated transducer, the mirror fulfills its role and can efficiently trap waves in the piezoelectric film, as seen on the displacement distribution shown in Figure 8.26(b). In such conditions, the guided waves operate very close to Lamb waves and can therefore exhibit very large phase velocities. In [KON 10], a resonance frequency of 1.83 GHz was reached using a mode similar to the S_1 Lamb mode in a piezoelectric plate, for an electrode period of $8.4 \mu\text{m}$.

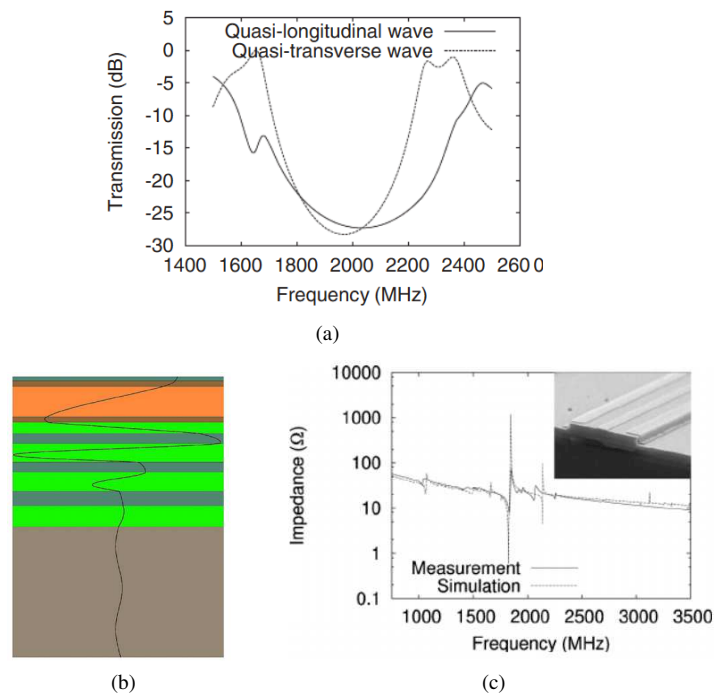


Figure 8.26. Resonators exploiting waves guided in an aluminum nitride film on top of an SiN/SiOC Bragg mirror [KON 10]: (a) transmission coefficient for longitudinal and shear waves of the Bragg reflector, (b) sketch of the layer stack and of the vertical displacement field versus depth of the mode of interest and (c) electric response (inset, a scanning electron microscopy image of the resonator) of the resonator (solid) along with the simulated response (dashed)

Despite reaching high frequencies, the resonators obtained in these initial works suffered from relatively low electromechanical coupling factors (respectively 0.75% and 2%). This made them inappropriate for the synthesis of front-end filters. The reason for such low electromechanical coupling factors originated from the fact that Lamb waves in aluminum nitride, which was considered as the piezoelectric film in these two works, exhibit naturally relatively weak electromechanical coupling factor. This material performs better for bulk wave resonators. For this reason, Takai *et al.* [TAK 16] investigated rather the use of lithium tantalate as the piezoelectric material, since it benefits from increased piezoelectric properties compared to aluminum nitride. This material cannot be readily deposited, but a thin monocrystalline film of LiTaO_3 can be transferred on a supporting substrate as an alternative. Takai *et al.* used this technology to transfer such a film on top of a Bragg mirror made of silicon dioxide and aluminum nitride or silicon nitride, to fabricate resonators and filters operating at 1.9 GHz. The low intrinsic losses of lithium tantalate, added to the high confinement of waves brought by the acoustic reflector, provided quality factors close to 4,000, that is, three times larger than conventional SAW devices fabricated on a bulk lithium tantalate substrate. Moreover, inserting silicon dioxide in the resonator, a material that, unlike nearly any other, has the extremely interesting property of having a stiffness increasing with temperature, offers some significant compensation of the frequency drifts with temperature. The cumulation of these three important parameters for the synthesis of high-performance filters has caused this solution to be dubbed “incredibly high-performance SAW” and made it currently a hot topic in the filter community.

Still, one-dimensional superlattices, or Bragg mirrors, cannot be fully related to phononics. The literature however features some higher-dimensional examples of particularly well-suited applications of phononic crystals to SAW resonators. The most elegant approach has been proposed by Solal *et al.* [SOL 10a] to solve the issue related to parasitic resonances appearing in SAW resonators due to diffraction effects in the electrode gratings and causing lateral standing waves, which perturb the electric response of resonators. These phenomena degrade the quality factor of these components, which translates into additional transmission losses for a filter. To prevent their formation, the authors proposed to add a second periodicity to the initial one inherited from the periodic electrode strips. This takes the form of tungsten plugs added periodically on top of the interdigitated electrodes of resonators, as sketched in Figure 8.27(a). This two-dimensional periodic structure opens a band gap, which then prevents the propagation of waves in the direction perpendicular to the expected surface waves, and as such improves the quality factor of SAW resonators, which manifests in the decrease of the minimum impedance level in Figure 8.27(b). With a very close approach, Yantchev and Plessky [YAN 13] considered acoustic diffraction not only inside the electrode gratings as a source of losses in SAW resonators but also towards the outside of the resonators. These sources of leakage arise from the natural diffraction occurring due to the finite length of the electrodes as well as because at their ends the electrodes face the opposite bus bar, so that the local electric

field perpendicular to the expected propagation direction causes the excitation of laterally propagating waves. To prevent these losses, they also propose to add plugs over the bus bars of the SAW resonators. Their work has so far only remained theoretical, and for the moment, industrial SAW filters do not seem to embed phononic structures for parasitic resonances suppression.

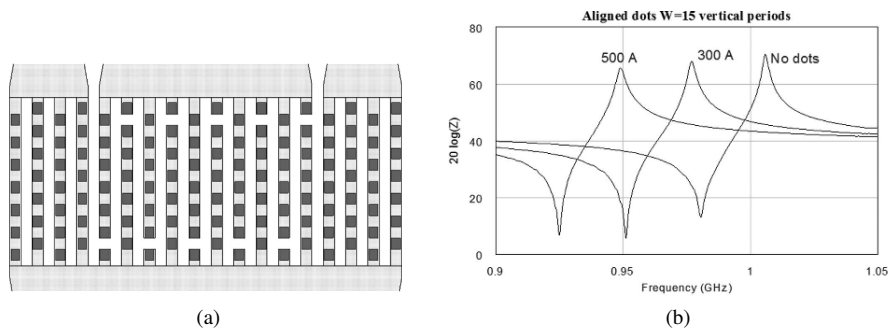


Figure 8.27. Phononic crystal made of *W* plugs positioned on top of the electrodes of a SAW resonator [SOL 10a]: (a) sketch of the modification of a conventional SAW resonator and (b) electric response vs. thickness of the plugs

8.4.3. Phononics for photonics

As a last field of application, a striking feature of Figure 8.1 is that hypersonic waves exhibit the same wavelengths as optical waves. Optical communications are another way to transmit data in addition to air propagation. The fact that radiofrequency acoustic waves share the same wavelengths as optical waves, and can therefore interact at the wavelength level, offers one way of manipulating optical waves with radiofrequency signals.

Interaction of light with elastic waves, however, occurs independently of the commensurability of their respective wavelength. The most widespread component illustrating this is the acousto-optical modulator: the strain produced by an elastic wave causes periodic variations of the refractive index of the medium that affects the propagation of optical waves, usually by acting like a time-dependent diffraction grating. These perturbations being also time-periodic cause a modulation of the optical signal and are widely used in acousto-optical modulators. Commercial acousto-optical modulators are based on interactions occurring in a bulk substrate, with a transduction piezoelectric layer usually separated from the propagation medium. Attempts to transpose the concept of these devices to integrated optical systems have been reported in the literature. The proposed integrated modulators rely

on surface acoustic waves to provide the necessary strain, due to their ease of fabrication and the natural confinement of strain close to the surface of the substrates where optical waveguides can be easily implemented. If diffraction efficiencies close to one could be reached [TSA 13], efficiency of the acousto-optical coupling is however relatively low and requires very long interaction length and high input acoustic power to achieve satisfying performances. The concepts and capabilities offered by the advent of photonic and phononic crystals appeared as potential ways to circumvent these limitations. Tailoring the dispersion properties of optical waves with photonic crystals has, for instance, led to the concept of *slow light*, when the group velocity of optical waves can be strongly decreased by the bending of dispersion curves close to the edges of the photonic band gap. This calls for largely increased interaction times with the perturbation source, either electro-optic [ROU 06, BRO 08] or acousto-optic [RUS 03, LIM 05, COU 10]. Even stronger interaction is expected when the interaction between elastic strains and electromagnetic fields is exacerbated by a simultaneous confinement of the acoustic and optical waves in a phononic/photonic waveguide or cavity. This fact was first observed in one-dimensional superlattices [TRI 02], and then evidenced in specifically designed photonic crystal fibers [KAN 09] or cavities [FUH 11]. It has then motivated the research for crystals simultaneously exhibiting band gaps for optical and elastic waves, also dubbed *phoxonic crystals*.

Maldovan and Thomas theoretically demonstrated that complete photonic and phononic band gaps can open in infinite two-dimensional square or hexagonal lattices of holes [MAL 06a]. They also showed that such crystals could be used to provide simultaneous confinement of elastic and optical waves in cavities [MAL 06b]. Later, Pennec *et al.* [PEN 10] and Mohammadi *et al.* [MOH 10] demonstrated that this is also possible in silicon slabs drilled with circular air holes forming a honeycomb lattice for high filling fractions. They demonstrated that other arrangements lead to gaps only valid for some specific polarizations of light. El Hassouani *et al.* demonstrated that arrays of silicon pillars formed on top of a silicon dioxide slab, on their side, can exhibit complete phoxonic band gaps for any type of lattice [ELH 10].

The field enhancement expected by a joint confinement of light and sound also opens appealing perspectives in the fast expanding field of *optomechanics*. Optomechanics is based on the use and enhancement of the interaction between optical radiation-pressure forces and mechanical motion. This interaction was initially exploited to achieve ground-state cooling for ions in ultracold atom experiments and has since then shown its potential for coherent control of the mechanical motion of micro- or nanoscale objects with relatively large masses, hence setting an exciting playground for, among others, the realization of tabletop quantum experiments [ASP 14]. In some cases, radiation-pressure forces can be seen as a relevant way to replace the conventional piezoelectric or electrostatic transduction for nanostructures, since these schemes do not scale favorably when dimensions become smaller, while optical forces become significant for low-mass objects. This,

associated with the intrinsic contactless nature of this transduction scheme, in the sense that no electrodes are required at the level of the resonator, makes it particularly suited to ultrasensitive mechanical sensing [KRA 12]. As a now fairly standard scheme for such an experiment, Li *et al.* excited the vibration of a freestanding clamped–clamped silicon beam using the electromagnetic radiation forces generated by the proximity with an optical waveguide and probed the displacement of this resonator through an evanescent coupling between the optical waveguide and the nano-beam [LI 08]. One of the first applications of this readout scheme is optical modulation: the displacements of the resonator induced by the optical forces induces a time-varying geometrical configuration, which in turns translates in tuning the photonic circuits [ROS 09]. In the opposite way: through the interplay of the mechanical nonlinearities, which are naturally strong in nanoscale mechanical structures, the optical forces can oppose in some configuration the motion of the mechanical structure and quench it. This allows us to counteract the natural motion of a nano-mechanical structure caused by the thermal phonon bath, and is therefore called *optical cooling* [ARC 06].

All these applications require high-quality-factor mechanical and optical structures to convert the relatively weak forces into large displacements, or to benefit from a naturally weak coupling to the thermal phonon bath [FON 10]. Such high quality factors are achieved by a proper choice of material with low damping (silicon, or strained silicon nitride [FON 10]), as well as with a beam structure capable of offering a strong localization for the optical and mechanical modes. This is where phoxonic crystals come into play. In [EIC 09], the crystal takes the form of a one-dimensional crystal with a ladder shape, obtained by etching almost rectangular holes along the length of a silicon nano-beam. Several designs combining phononic crystal-based acoustic shielding and one- and two-dimensional optomechanical cavities were then proposed and implemented [SAF 10, CHA 12]. More recent structures rely now on a combination of strain engineering and mechanical decoupling from the surroundings of the resonator. Engineering strain consists in tapering the nano-beam to concentrate stress up to the material yield strength in the region where waves will be localized. When in high tension, the material is made stiffer, which strongly decreases its mechanical damping. Mechanical decoupling is achieved by adding a phononic crystal to suppress anchor losses, as was proposed for MEMS resonators. To accommodate for the dispersion induced by the tapering of the beam, the phoxonic crystal, taking the form of stubs added to the edges of the beam, is also tapered, as shown in Figure 8.28. Such an exquisite arrangement manages to provide elastic modes with quality factor times frequency products in the range of 10^{15} Hz at room temperature, which is an order of magnitude higher than the best electromechanical resonators reported to date. The perspectives opened by such high quality factors are resonators with extremely long phonon coherence time and with a sufficiently low number of thermal phonons to reveal quantum elastic effects in relatively large mechanical objects without the need to go towards cryogenic temperatures.



Figure 8.28. Nano-mechanical beam resonator benefiting from strain engineering and from a phononic crystal to increase the phonon coherence time [GHA 18]

From a shorter-term perspective, optomechanical systems have proved relevant for the realization of radiofrequency signal processing devices, given the intrinsic information transfer occurring between the optical and the RF or microwave domains in such physical systems. A practical implementation to the field of information and communication technologies however requires a higher level of integration that can be reached by integrating an electrical or piezoelectrical actuation scheme to the opto-mechanical system in order to drive the mechanical motion through external, stronger, coherent RF driving fields. These optomechanical on-chip devices have received growing interest over the past few years, and tend to integrate a rising number of functionalities and degrees of freedom for both the RF and the optical regimes [WIN 11, BOC 13, XIO 13]. If a complete integration of simultaneous photonic and phononic crystals or cavities in such systems is still to be unambiguously demonstrated, then strategies based on the association of a photonic nanobeam with a phononic waveguide have been used to show that both optical and mechanical excitation and readout of the RF signal could be achieved [BAL 16]. Interestingly, the proposed architecture integrates interdigitated transducers operating at 2.4 GHz, a configuration that brings the proposed device closer to more classical piezoelectric RF components and paves the way to an integrated circuitry supporting traveling elastic waves, broadening the already wide avenues opened by recent developments in nano-opto-electromechanical systems [MID 18]. Whether elastic metamaterials will be considered as presenting enough added-value to be integrated in already complex systems is still an open discussion.

8.5. Perspectives

The applications of phononic crystals, or more generally of elastic metamaterials, to radiofrequency applications is a perfect example of adoption of a new technology following the *hype cycle* developed by the research and advisory firm Gartner, shown in Figure 8.29.

Starting with early works on phononic crystals as a *technology trigger*, initial expectations were the possibility of introducing phononic chips built upon phononic waveguide circuits and achieving complex functions devoted to wave manipulations,

which would outperform RF electronics with a tremendous level of miniaturization. Early developments led in the early 2000s indeed demonstrated the possibility of implementing phononic crystals operating in the hypersonic regime and compatible with already existing acoustic resonator structures such as SAW or BAW devices. The confidence grew when waveguides, stubbed structures and resonant cavities were demonstrated, until reaching a *peak of inflated expectations* in the early 2010s. It however soon became evident that the specifications that could be expected from phononic structures were far behind the needs of RF communications systems, which were already pushing mature technologies such as SAW or BAW devices to extremes. Waveguides suffered from utterly large losses; reflectors, although compact, did not provide a better confinement than existing solutions and even induced more complexity and caused additional design concerns. Even the adoption of phononic crystals as replacement for resonator anchors by the MEMS community did, generally speaking, not fulfill expectations. The *trough of disillusionment* was reached.

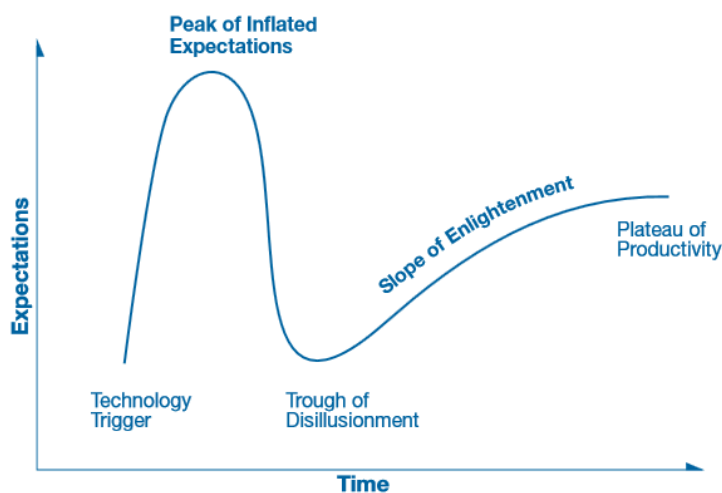


Figure 8.29. Graphical representation of the hype cycle [GAR 16]

There are some clues that the *slope of enlightenment* may be the current state for radiofrequency elastic metamaterials, although one can only look backwards to evaluate a position on a hype cycle *a posteriori*. As discussed in section 8.4.2, some applications are still under investigation for SAW devices: the current interest in incredibly high-performance SAW filters may be a sign, although these devices have not yet entered in mass production as promised in the end of 2016 [TAK 16].

AQ2 We can also briefly mention some ongoing works for integration of mechanical resonators within integrated circuits [BAR 15], with the goal of delivering miniaturized timing functions directly at the core of circuits, or to provide mechanical signal processing, which could lower power consumption compared to the same functions achieved using transistors. Such mechanical devices, being solidly embedded inside the transistor that interconnects solid structures, have to rely on hypersonic crystals such as the ones described in Figure 8.12a. More generally, the field of *acoustoelectronics*, that is the manipulation of electrons by acoustic waves propagating in semiconductor materials, or the perturbation of transistors (e.g. the modulation of their gate voltage) by a radiofrequency wave is also currently a growing field of interest.

The fields of phoxonics or optomechanics described in section 8.4.3 are also full of promises. Such structures could benefit optical telecommunications, as well as high-sensitivity sensors and quantum information processing. Mechanical confinement has proved to be a necessary ingredient of these optomechanical systems and may provide an application field for elastic metamaterials. In addition to actuation through radiation-pressure forces, the recent reports of optomechanical platforms involving coherent elastic wave source in the GHz range have triggered some interest in the community of quantum electromechanics. Inspired by the use of surface acoustic wave devices in semiconductor physics as charge and spin carriers [HER 11, MCN 11], the field of circuit quantum electrodynamics (CQED), defined as the solid-state equivalent of QED, has started adopting SAW [GUS 14] and BAW [CHU 17] devices as the source of the mechanical motion to be coupled with superconducting qubits. In this context, operating at GHz frequencies and with mechanical cavities with high quality factors is key, which may revive interest for hypersonic phononic cavities.

8.6. References

- [ACH 11] ACHAQUI Y., KHELIF A., BENCHABANE S. *et al.*, “Experimental observation of locally-resonant and Bragg band gaps for surface guided waves in a phononic crystal of pillars”, *Physical Review B*, vol. 83, p. 104201, American Physical Society, March 2011.
- [ARC 06] ARCIZET O., COHADON P.-F., BRIANT T. *et al.*, “Radiation-pressure cooling and optomechanical instability of a micro-mirror”, *Nature*, vol. 444, p. 71, 2006.
- [ASH 17] ASH B.J., WORSFOLD S.R., VUKUSIC P. *et al.*, “A highly attenuating and frequency tailorable annular hole phononic crystal for surface acoustic waves”, *Nature Communications*, vol. 8, p. 174, 2017.
- [ASP 14] ASPELMEYER M., KIPPENBERG T.J., MARQUARDT F., “Cavity optomechanics”, *Reviews of Modern Physics*, vol. 86, pp. 1391–1452, American Physical Society, December 2014.

- [ASS 08] ASSOUAR B.M., VINCENT B. MOUBCHIR H., “Phononic crystals based on LiNbO_3 realised using domain inversion by electron-beam irradiation”, *IEEE Transactions on Ultrasonics, Ferroelectrics, and Frequency Control*, vol. 55, no. 2, pp. 273–278, 2008.
- [BAL 16] BALRAM K.C., DAVANCO M.I., SONG J.D. *et al.*, “Coherent coupling between radiofrequency, optical and acoustic waves in piezo-optomechanical circuits”, *Nature Photonics*, vol. 10, pp. 346–352, 2016.
- [BAR 98] BARTELS A., DEKORSY T., KURZ H. *et al.*, “Coherent control of acoustic phonons in semiconductor superlattices”, *Applied Physics Letters*, vol. 72, p. 2844, 1998.
- [BAR 15] BAR B., MARATHE R., WEINSTEIN D., “Theory and design of phononic crystals for unreleased CMOS-MEMS resonant body transistors”, *Journal of Microelectromechanical systems*, vol. 24, pp. 1520–1533, 2015.
- [BEN 06] BENCHABANE S., KHELIF A., RAUCH J. *et al.*, “Evidence for complete surface wave band gap in a piezoelectric phononic crystal”, *Physical Review E*, vol. 73, p. 065601, 2006.
- [BEN 15] BENCHABANE S., GAIFFE O., SALUT R. *et al.*, “Guidance of surface waves in a micron-scale phononic crystal line-defect waveguide”, *Applied Physics Letters*, vol. 106, p. 081903, 2015.
- [BOC 13] BOCHMANN J., VAINSENER A., AWSCHALOM D.D. *et al.*, “Nanomechanical coupling between microwave and optical photons”, *Nature Physics*, vol. 9, pp. 712–716, 2013.
- [BOE 13] BOEHLER N., ELIASON J.K., KUMAR A. *et al.*, “Interaction of a contact resonance of microspheres with surface acoustic waves”, *Physical Review Letters*, vol. 111, p. 036103, American Physical Society, July 2013.
- [BRO 08] BROSI J.-M., KOOS C., ANDREANI L.C. *et al.*, “High-speed low-voltage electro-optic modulator with a polymer-infiltrated silicon photonic crystal waveguide”, *Optics Express*, vol. 16, no. 6, pp. 4177–4191, OSA, Mar 2008.
- [CAM 14] CAMPANELLA H., WANG N., NARDUCCI M. *et al.*, “Integration of RF MEMS resonators and phononic crystals for high frequency applications with frequency-selective heat management and efficient power handling”, *2014 International Electron Device Meeting*, pp. 566–569, 2014.
- [CHA 12] CHAN J., SAFAVI-NAEINI A.H., HILL J.T. *et al.*, “Optimized optomechanical crystal cavity with acoustic radiation shield”, *Applied Physics Letters*, vol. 101, no. 8, p. 081115, 2012.
- [CHI 10] CHIANG Y.-F., SUNG C.-C., RO R., “Effects of metal buffer layer on characteristics of surface acoustic waves in ZnO/metal/diamond structures”, *Applied Physics Letters*, vol. 96, p. 154104, 2010.
- [CHU 17] CHU Y., KHAREL P., RENNINGER W.H. *et al.*, “Quantum acoustics with superconducting qubits”, *Science, American Association for the Advancement of Science*, 2017.
- [COU 10] COURJAL N., BENCHABANE S., DAHDAH J. *et al.*, “Acousto-optically tunable lithium niobate photonic crystal”, *Applied Physics Letters*, vol. 96, p. 131103, 2010.

- [CUF 12] CUFFE J., CHAVEZ E., SHCHEPETOV A. *et al.*, “Phonons in slow motion: Dispersion relations in ultrathin Si membranes”, *Nano Letters*, vol. 12, pp. 3569–3573, 2012.
- [DEF 01] DEFRANOULD P., WRIGHT P., “Filtres à ondes de surface”, *Techniques de l’Ingénieur*, Editions TI, 2001.
- [DHA 00] DHAR L., ROGERS J.A., “High frequency one-dimensional phononic crystal characterized with a picosecond transient grating photoacoustique technique”, *Applied Physics Letters*, vol. 77, p. 1402, 2000.
- [DIE 01] DIEULESAINT E., ROYER D., “Dispositifs acousto-électroniques”, *Techniques de l’Ingénieur*, Editions TI, 2001.
- [EIC 09] EICHENFIELD M., CHAN J., COMACHO R.M. *et al.*, “Optomechanical crystals”, *Nature*, vol. 462, p. 78, 2009.
- [ELH 10] EL HASSOUANI Y., LI C., PENNEC Y. *et al.*, “Dual phononic and photonic band gaps in a periodic array of pillars deposited on a thin plate”, *Physical Review B*, vol. 82, p. 155405, 2010.
- [ELI 16] ELIASON J., VEGA-FLICK A., HIRAIWA M. *et al.*, “Resonant attenuation of surface acoustic waves by a disordered monolayer of microspheres”, *Applied Physics Letters*, vol. 108, p. 061907, 2016.
- [FON 10] FONG K.Y., PERNICE H.P., LI M. *et al.*, “High Q optomechanical resonators in silicon nitride nanophotonic circuits”, *Applied Physics Letters*, vol. 97, p. 073112, 2010.
- [FUH 11] FUHRMANN D.A., THON S.M., KIM H. *et al.*, “Dynamic modulation of photonic crystal nanocavities using gigahertz acoustic phonons”, *Nature Photonics*, vol. 5, pp. 605–609, 2011.
- AQ4 [GAR 16] Gartner, Inside Gartner Research, 2016.
- [GHA 18] GHADIMI A.H., FEDOROV S.A., ENGELSEN N.J. *et al.*, “Elastic strain engineering for ultralow mechanical dissipation”, *Science*, vol. 360, pp. 764–768, 2018.
- [GOR 05] GORISHNYI T., ULLAL C., MALDOVAN M. *et al.*, “Hypersonic phononic crystals”, *Physical Review Letters*, vol. 94, p. 115501, March 2005.
- [GOR 11] GORISSE M., BENCHABANE S., TEISSIER G. *et al.*, “Observation of band gaps in the GHz range and deaf bands in a hypersonic aluminium nitride phononic crystal slab”, *Applied Physics Letters*, vol. 98, p. 234103, 2011.
- [GRA 12] GRACZYKOWSKI B., MIELCAREK S., TRZASKOWSKA A. *et al.*, “Tuning of a hypersonic surface phononic band gap using a nanoscale two-dimensional lattice of pillars”, *Physical Review B*, vol. 86, p. 085426, 2012.
- [GUS 14] GUSTAFSSON M.V., AREF T., KOCKUM A.F. *et al.*, “Propagating phonons coupled to an artificial atom”, *Science*, vol. 346, no. 6206, pp. 207–211, American Association for the Advancement of Science, 2014.
- [HAG 72] HAGON P.J., DYAL L., LAKIN K.M., “Wide band UHF compression filters using aluminum nitride on sapphire”, *Proceedings of the 1972 IEEE Ultrasonics Symposium*, pp. 274–275, 1972.

- [HER 11] HERMELIN S., TAKADA S., YAMAMOTO M. *et al.*, “Electrons surfing on sound wave as a platform for quantum optics with flying electrons”, *Nature*, vol. 477, pp. 435–438, 2011.
- [HIR 16] HIRAIWA M., ABI GHANEM M., WALLEEN S.P. *et al.*, “Complex contact-based dynamics of microsphere monolayers revealed by resonant attenuation of surface acoustic waves”, *Physical Review Letters*, vol. 116, p. 198001, American Physical Society, May 2016.
- [HSI 07] HSIAO F.-L., KHELIF A., MOUBCHIR H. *et al.*, “Complete band gaps and deaf bands of triangular and honeycomb water-steel phononic crystals”, *Journal of Applied Physics*, vol. 101, p. 044903, 2007.
- [HSU 06] HSU J.-C., WU T.-T., “Efficient formulation for band-structure calculations of two-dimensional phononic crystal plates”, *Physical Review B*, vol. 74, p. 144303, 2006.
- [HSU 07a] HSU J.-C., WU T.-T., “Lamb waves in binary locally resonant phononic plates with two-dimensional lattices”, *Applied Physics Letters*, vol. 90, p. 201904, 2007.
- [HSU 07b] HSU J.-C., WU T.-T., “Analysis of Lamb-wave dispersion and band gaps of two-dimensional piezoelectric phononic-crystal plates”, *Proceedings of the 2007 IEEE Ultrasonics Symposium*, pp. 624–627, 2007.
- [JAN 11] JANSEN R., STOFFELS S., ROTTENBERG X. *et al.*, “Optimal T-support anchoring for BAR-type BAW resonators”, *MEMS 2011*, pp. 609–612, 2011.
- [KAF 00] KAFESAKI M., SIGALAS M., GARCIA N., “Frequency modulation in the transmittivity of wave guides in elastic-wave band-gap materials”, *Physical Review Letters*, vol. 85, pp. 4044–4047, 2000.
- [KAN 09] KANG M.S., NAZARKIN A., BRENN A. *et al.*, “Tightly trapped acoustic phonons in photonic crystal fibres as highly nonlinear artificial Raman oscillators”, *Nature Physics*, vol. 5, pp. 276–280, 2009.
- [KHE 02] KHELIF A., DJAFARI-ROUHANI B., VASSEUR J. *et al.*, “Transmittivity through straight and stublike waveguides in a two-dimensional phononic crystal”, *Physical Review B*, vol. 65, p. 174308, 2002.
- [KHE 03] KHELIF A., CHOUJAA A., DJAFARI-ROUHANI B. *et al.*, “Trapping and guiding of acoustic waves by defect modes in a full-band-gap ultrasonic crystal”, *Physical Review B*, vol. 68, p. 214301, 2003.
- [KHE 04] KHELIF A., CHOUJAA A., BENCHABANE S. *et al.*, “Guiding and bending of acoustic waves in highly confined phononic crystal waveguides”, *Applied Physics Letters*, vol. 84, p. 4400, 2004.
- [KHE 08] KHELIF A., CHOUJAA A., RAUCH J.-Y. *et al.*, “The OmniSAW device concept”, *IEEE Ultrasonics Symposium*, 2008.
- [KHE 10a] KHELIF A., ACHAOUY Y., BENCHABANE S. *et al.*, “Locally resonant surface acoustic wave band gaps in a two-dimensional phononic crystal of pillars on a surface”, *Physical Review B*, vol. 81, p. 214303, 2010.

- [KHE 10b] KHELIF A., MOHAMMADI S., EFTEKHAR A.A. *et al.*, “Acoustic confinement and waveguiding with a line-defect structure in phononic crystal slabs”, *Journal of Applied Physics*, vol. 108, p. 084515, 2010.
- [KOK 07] KOKKONEN K., KAIVOLA M., BENCHABANE S. *et al.*, “Scattering of surface acoustic waves by a phononic crystal revealed by heterodyne interferometry”, *Applied Physics Letters*, vol. 91, p. 083517, 2007.
- [KON 10] KONÉ I., DOMINGUE F., REINHARDT A. *et al.*, “Guided acoustic wave resonators using an acoustic Bragg mirror”, *Applied Physics Letters*, vol. 96, p. 223504, 2010.
- [KRA 12] KRAUSE A.G., WINGER M., BLASIUS T.D. *et al.*, “A high-resolution microchip optomechanical accelerometer”, *Nature Photonics*, vol. 6, pp. 768–772, 2012.
- [KUO 11] KUO N.-K., PIAZZA G., “1 GHz phononic band gap structure in air/aluminum nitride for symmetric Lamb waves”, *MEMS 2011*, pp. 740–743, 2011.
- [LAU 05] LAUDE V., WILM M., KHELIF A. *et al.*, “Full band gap for surface acoustic waves in a piezoelectric phononic crystal”, *Physical Review E*, vol. 71, p. 036607, 2005.
- [LI 08] LI M., PERNICE W. H.P., XIONG C. *et al.*, “Harnessing optical forces in integrated photonic circuits”, *Nature*, vol. 456, pp. 480–484, 2008.
- [LIM 05] DE LIMA JR M.M., SANTOS P.V., “Modulation of photonic structures by surface acoustic waves”, *Reports on Progress in Physics*, vol. 68, no. 7, p. 1639, 2005.
- [LIU 14] LIU T.-W., TSAI Y.-C., LIN Y.-C. *et al.*, “Design and fabrication of a phononic-crystal-based Love wave resonator in GHz range”, *AIP Advances*, vol. 4, p. 124201, 2014.
- [MAL 06a] MALDOLVAN M., THOMAS E.L., “Simultaneous complete elastic and electromagnetic band gaps in periodic structures”, *Applied Physics B*, vol. 83, p. 595, 2006.
- [MAL 06b] MALDOLVAN M., THOMAS E.L., “Simultaneous localization of photons and phonons in two-dimensional periodic structures”, *Applied Physics Letters*, vol. 88, p. 251907, 2006.
- AQ5 [MAR 05] MARKSTEINER S., KAITILA J., FATTINGER G.G. *et al.*, “Optimization of acoustic mirrors for solidly mounted BAW resonators”, *Proceedings of the IEEE Ultrasonics Symposium*, vol. 1, pp. 329–332, 2005.
- [MAY 91] MAYER P.A., ZIERAU W., MARADUDIN A., “Surface acoustic waves propagating along the grooves of a periodic grating”, *Journal of Applied Physics*, vol. 69, pp. 1942–1947, 03 1991.
- [MCN 11] MCNEIL R.P.G., KATAOKA M., FORD C.J.B. *et al.*, “On-demand single-electron transfer between distant quantum dots”, *Nature*, vol. 477, pp. 439–442, 2011.
- [MID 18] MIDOLO L., SCHLIESSER A., FIORE A., “Nano-opto-electro-mechanical systems”, *Nature Nanotechnology*, vol. 13, pp. 11–18, 2018.
- [MOH 08] MOHAMMADI S., EFTEKHAR A.A., KHELIF A. *et al.*, “Evidence of large high frequency complete phononic band gaps in silicon phononic crystal plates”, *Applied Physics Letters*, vol. 92, p. 221905, 2008.
- [MOH 09] MOHAMMADI S., EFTEKHAR A.A., HUNT W.D. *et al.*, “High-Q micromechanical resonators in a two-dimensional phononic crystal slab”, *Applied Physics Letters*, vol. 94, p. 051906, 2009.

- [MOH 10] MOHAMMADI S., EFTEKHAR A.A., KHELIF A. *et al.*, “Simultaneous two-dimensional phononic and photonic band gaps in opto-mechanical crystal slabs”, *Optics Express*, vol. 18, p. 9164, 2010.
- [MOH 11] MOHAMMADI S., EFTEKHAR A.A., POURABOLGHAEM R. *et al.*, “Simultaneous high-Q confinement and selective direct piezoelectric excitation of flexural and extensional lateral vibrations in a silicon phononic crystal slab resonator”, *Sensors and Actuators A: Physical*, vol. 167, 2011.
- [NEW 65] NEWELL W., “Face-mounted piezoelectric resonators”, *Proceedings of the IEEE*, vol. 53, pp. 575–581, 1965.
- [OLS 07] OLSSON R.H., FLEMING J.G., EL-KADY I.F. *et al.*, “Micromachined bulk wave acoustic bandgap devices”, *Transducers and Eurosensors '07*, pp. 317–321, 2007.
- [OLS 09] OLSSON R.H., EL-KADY I., “Microfabricated phononic crystal devices and applications”, *Measurement Science and Technology*, vol. 20, p. 012002, 2009.
- [OSE 18] OSEEV A., MUKHIN N.V., LUCKLUM R. *et al.*, “Towards macroporous phononic crystal based structures for FBAR applications. Theoretical investigation of technologically competitive solutions”, *Microsystem Technologies*, vol. 24, pp. 2389–2399, 2018.
- [OUD 10] OUDICH M., ASSOUAR M.B., HOU Z., “Propagation of acoustic waves and waveguiding in a locally resonant phononic crystal plate”, *Applied Physics Letters*, vol. 97, p. 193503, 2010.
- [OZG 01] OZGUR U., LEE C.-W., EVERITT H.O., “Control of coherent acoustic phonons in semiconductor quantum wells”, *Physical Review Letters*, vol. 86, p. 5604, 2001.
- [PEN 05] PENNEC Y., DJAFARI-ROUHANI B., VASSEUR J. *et al.*, “Acoustic channel drop tunneling in a phononic crystal”, *Applied Physics Letters*, vol. 87, p. 261912, 2005.
- [PEN 08] PENNEC Y., DJAFARI-ROUHANI B., LARABI H. *et al.*, “Low-frequency gaps in a phononic crystal constituted of cylindrical dots deposited on a thin homogeneous plate”, *Physical Review B*, vol. 78, p. 104105, 2008.
- [PEN 10] PENNEC Y., DJAFARI-ROUHANI B., EL BOUDOUTI E.H. *et al.*, “Simultaneous existence of phononic and photonic band gaps in periodic crystal slabs”, *Optics Express*, vol. 18, p. 14301, 2010.
- [QIN 16] QIN P., ZHU H., LEE J. E.-Y. *et al.*, “Phase noise reduction in a VHF MEMS-CMOS oscillator using phononic crystals”, *Journal of the Electron Devices Society*, vol. 4, p. 149, 2016.
- [ROS 09] ROSENBERG J., LIN Q., PAINTER O., “Static and dynamic wavelength routing via the gradient optical force”, *Nature Photonics*, vol. 3, pp. 478–483, 2009.
- [ROU 06] ROUSSEY M., BERNAL M.-P., COURJAL N. *et al.*, “Electro-optic effect exaltation on lithium niobate photonic crystals due to slow photons”, *Applied Physics Letters*, vol. 89, p. 241110, 2006.
- [RUS 03] RUSSELL P.S.J., MARIN E., DÍEZ A. *et al.*, “Sonic band gaps in PCF preforms: Enhancing the interaction of sound and light”, *Optics Express*, vol. 11, no. 20, pp. 2555–2560, OSA, October 2003.

- [SAF 10] SAFAVI-NAEINI A.H., PAINTER O., “Design of optomechanical cavities and waveguides on a simultaneous bandgap phononic-photonic crystal slab”, *Optics Express*, vol. 18, no. 14, pp. 14926–14943, OSA, July 2010.
- [SOC 12] SOCIÉ L., BENCHABANE S., ROBERT L. *et al.*, “SAW waveguiding in high aspect ratio transducers”, *2012 IEEE International Ultrasonics Symposium*, pp. 1794–1797, October 2012.
- [SOL 10a] SOLAL M., GRATIER J., KOOK T., “A SAW resonator with two-dimensional reflectors”, *IEEE Transactions on Ultrasonics, Ferroelectrics, and Frequency Control*, vol. 57, pp. 30–37, 2010.
- [SOL 10b] SOLIMAN Y., SU M., LESEMAN Z. *et al.*, “Phononic crystals operating in the gigahertz range with extremely wide band gaps”, *Applied Physics Letters*, vol. 97, p. 193502, 2010.
- [SOR 11] SORENSON L., FU J.L., AYAZI F., “One-dimensional linear acoustic bandgap structures for performance enhancement of AlN-on-Silicon micromechanical resonators”, *2011 16th International Solid-State Sensors, Actuators and Microsystems Conference*, pp. 918–921, 2011.
- [SUN 09] SUN J.-H., WU T.-T., “Lamb wave source based on the resonant cavity of phononic crystal plates”, *IEEE Transactions on Ultrasonics, Ferroelectrics, and Frequency Control*, vol. 56, p. 121, 2009.
- [SUN 10] SUN C.-Y., HSU J.-C., WU T.-T., “Resonant slow modes in phononic crystal plates with periodic membranes”, *Applied Physics Letters*, vol. 97, p. 031902, 2010.
- [TAK 16] TAKAI T., IWAMOTO H., TAKAMINE Y. *et al.*, “Incredible high performance SAW resonator on novel multi-layered substrate”, *Proceedings of IEEE Ultrasonics Symposium*, pp. 456–459, 2016.
- [TAL 06] TALHAMMER R., “Spurious mode suppression in BAW resonators”, *Proceedings of IEEE Ultrasonics Symposium*, pp. 456–459, 2006.
- [TAN 07] TANAKA A., YANAGITANI T., MATSUKAWA M. *et al.*, “Propagation characteristics of SH-SAW in (11-20) ZnO layer/silica glass substrate structure”, *Proceedings of 2007 IEEE Ultrasonics Symposium*, pp. 280–283, 2007.
- [TRI 02] TRIGO M., BRUCHHAUSEN A., FAINSTEIN A. *et al.*, “Confinement of acoustical vibrations in a semiconductor planar phonon cavity”, *Physical Review Letters*, vol. 89, p. 227402, 2002.
- [TSA 13] TSAI C., *Guided-Wave Acousto-Optics: Interactions, Devices, and Applications*, Springer Series in Electronics and Photonics, Springer Berlin Heidelberg, 2013.
- [TU 12] TU C., LEE J. E.-Y., “Increased dissipation from distributed etch holes in a lateral breathing mode silicon micromechanical resonator”, *Applied Physics Letters*, vol. 101, p. 023504, 2012.
- [WAN 15] WANG S., POPA L.C., WEINSTEIN D., “Tapered phononic crystal SAW resonator in GaN”, *Proceedings of 2015 IEEE MEMS Conference*, pp. 1028–1031, 2015.
- [WHI 65] WHITE R., WOLTMER F., “Direct piezoelectric coupling to surface elastic waves”, *Applied Physics Letters*, vol. 7, p. 314, 1965.

- [WIN 11] WINGER M., BLASIUS T.D., ALEGRE T.P.M. *et al.*, “A chip-scale integrated cavity-electro-optomechanics platform”, *Optics Express*, vol. 19, no. 25, pp. 24905–24921, OSA, December 2011.
- [WU 04] WU T.-T., HUANG Z.-G., LIN S., “Surface and bulk acoustic waves in two-dimensional phononic crystal consisting of materials with general anisotropy”, *Physical Review B*, vol. 69, p. 094301, 2004.
- [WU 05a] WU T.-T., HSU Z.-C., HUANG Z.-G., “Band gaps and the electromechanical coupling coefficient of a surface acoustic wave in a two-dimensional piezoelectric phononic crystal”, *Physical Review B*, vol. 71, p. 064303, 2005.
- [WU 05b] WU T.-T., WU L.-C., HUANG Z.-G., “Frequency band-gap measurement of two-dimensional air/silicon phononic crystals using layered slanted finger interdigital transducers”, *Journal of Applied Physics*, vol. 97, p. 094916, 2005.
- [WU 09] WU T.-T., WANG W.-S., SUN J.-H. *et al.*, “Utilization of phononic crystal reflective gratings in a layered surface acoustic wave device”, *Applied Physics Letters*, vol. 94, p. 101913, 2009.
- [WU 16] WU G., ZHU Y., MERUGU S. *et al.*, “GHz spurious mode free AlN Lamb wave resonator with high figure of merit using one dimensional phononic crystal tethers”, *Applied Physics Letters*, vol. 109, p. 013506, 2016.
- [XIO 13] XIONG C., FAN L., SUN X. *et al.*, “Cavity piezotomechanics: Piezoelectrically excited, optically transduced optomechanical resonators”, *Applied Physics Letters*, vol. 102, p. 021110, 2013.
- [YAM 08] YAMASHITA Y., HOSONO Y., “High effective lead perovskite ceramics and single crystals for ultrasonic imaging”, in HEYWANG W., LUBITZ K., WERSING W. (eds), *Piezoelectricity: Evolution and Future of a Technology*, Chapter 9, pp. 223–244, Springer, Berlin, 2008.
- [YAN 13] YANTCHEV V., PLESSKY V., “Analysis of two dimensional composite surface grating structures with applications to low loss microacoustic resonators”, *Journal of Applied Physics*, vol. 114, p. 074902, 2013.
- [YOL 17] Yole Développement, RF Front-End modules and components for cellphones, 2017.
- [YUD 12] YUDISTIRA D., PENNEC Y., DJAFARI-ROUHANI B. *et al.*, “Non-radiative complete SAW bandgap of 2D phononic crystals on semi-infinite LiNbO₃ substrate”, *Proceedings of the Acoustics 2012 Nantes Conference*, pp. 289–293, 2012.
- [YUD 16] YUDISTIRA D., BOES A., GRACZYKOWSKI B. *et al.*, “Nanoscale pillar hypersonic surface phononic crystals”, *Physical Review B*, vol. 94, p. 094304, American Physical Society, September 2016.



AQ1: Which chapters does this refer to?

AQ2: We have modified this sentence. Is it correct?

AQ3: Please provide full details

AQ4: Please provide full details

AQ5: Please check if this reference is okay.